

1 Gondwana break-up related magmatism in the Falkland Islands

2 M. J. Hole¹, R.M. Ellam², D.I.M. MacDonald¹ & S.P. Kelley³

3 ¹*Department of Geology & Petroleum Geology University of Aberdeen, AB24 3UE, UK*

4 ²*Scottish Universities Environment Research Centre, East Kilbride, Glasgow, G75 0QU, UK*

5 ³*Department of Earth & Environmental Sciences, Open University, Milton Keynes, MK7 6AA*
6 UK
7

8 Jurassic dykes (c. 182 Ma) are widespread across the Falkland Islands and exhibit considerable
9 geochemical variability. Orthopyroxene-bearing NW-SE oriented quartz-tholeiite dykes
10 underwent fractional crystallization > 1 GPa, and major element constraints suggest that they
11 were derived by melting of pyroxenite-rich source. They have ϵNd_{182} in the range -6 to -11 and
12 $^{87}\text{Sr}/^{86}\text{Sr}_{182} > 0.710$ and therefore require an old lithospheric component in their source. A suite
13 of basaltic-andesites and andesites exhibit geochemical compositions transitional between Ferrar
14 and Karoo magma types, and are similar to those seen in the KwaZulu-Natal region of southern
15 Africa and the Theron Mountains of Antarctica. Olivine-phyric intrusions equilibrated at < 0.5
16 GPa, and have isotopic compositions (ϵNd_{182} 1.6-3.6 and $^{87}\text{Sr}/^{86}\text{Sr}_{182}$ 0.7036-0.7058) that require
17 limited interaction with old continental lithosphere. A suite of plagioclase-phyric intrusions with
18 $^{87}\text{Sr}/^{86}\text{Sr}_{182}$ c. 0.7035 and ϵNd_{182} c. +4, and low Th/Ta and La/Ta ratios (c. 1 and c. 15
19 respectively) also largely escaped interaction with the lithosphere. These isotopically depleted
20 intrusions were probably emplaced synchronously with Gondwana fragmentation and the
21 formation of new oceanic lithosphere. Estimates of mantle potential temperature from olivine
22 equilibration temperatures do not provide unequivocal evidence for the presence of a plume
23 thermal anomaly beneath the Falkland Islands at 182 Ma.
24

25 The Early Jurassic (c. 180 Ma) Karoo and Ferrar large igneous provinces (LIP) were associated
26 with Gondwana break-up. Igneous rocks of the Karoo province occur predominantly in South
27 Africa but extend into Dronning Maud Land (Antarctica) with the main phase of activity taking
28 place in the interval 182-183 Ma (Svensen *et al.* 2012). The Ferrar Province, which is
29 contemporaneous with the magmatism in the Karoo province (Burgess *et al.* 2015), is typified
30 by the low TiO₂ Jurassic igneous rocks of the Transantarctic Mountains and Tasmania (Hergt *et*
31 *al.* 1989; Fleming *et al.* 1995). It has also been established that the Karoo and Ferrar provinces
32 have areas of geographical overlap, most notably in the KwaZulu area of South Africa (Sweeney
33 *et al.* 1994; Riley *et al.* 2006) and in the Theron Mountains of Antarctica (Brewer *et al.* 1992).
34 In the latter, at least four suites of low TiO₂ igneous rocks have been recognized, and it has been
35 suggested that there is a transition from one province to the other rather, than a strict
36 geographical delineation between the two provinces (Brewer *et al.* 1992).

37 Elliott & Fleming (2000) argued that the principal focus of magmatism for both the Karoo
38 and Ferrar provinces was the Weddell Triple Junction (Fig. 1) which was within the envelope of
39 a plume-related thermal anomaly associated with Gondwana break-up. Prior to Gondwana
40 fragmentation, plate reconstructions place the Falkland Islands on the extension of the Cape
41 Fold Belt of South Africa, on the eastern flank of the Lebombo Rift (Fig. 1; Macdonald *et al.*
42 2003; Stone *et al.* 2008; 2009; Richards *et al.* 2013). Post-180 Ma, there was major re-
43 organization of crustal blocks in Patagonia, the Falklands Plateau and west Antarctica, which
44 included the clockwise rotation of the Falklands crustal block in an overall extensional regime.
45 The 180° rotation of the Falkland Islands from their pre-180 Ma position was complete by 165
46 Ma (Macdonald *et al.* 2003), and by this time the islands had migrated to the west along the
47 extension of the Aghulas Fracture zone to a position well to the west of the WTJ (Richards *et al.*
48 2013). Consequently, the Falkland Islands may have been very close to the focus of break-up
49 related magmatism, and it is logical to assume that the geochemical composition of any igneous
50 rocks found in the islands should reflect the diversity of magmatism in the Jurassic Gondwana

51 LIP as a whole. In this paper, new data are presented that show that the dykes and minor
52 intrusions of the Falkland Islands exhibit variability in mineralogy, major element, trace element
53 and Sr-, Nd- and Pb-isotopic compositions that is nearly as large as that seen in the entire
54 Jurassic Gondwana LIP, even though the Falkland Islands themselves represent only an
55 extremely small area compared to the total distribution of Jurassic igneous rocks of the region.
56 Intrusions with major and trace element characteristics most similar the Ferrar dolerites of the
57 Transantarctic Mountain are juxtaposed with intrusions which are nearly identical to some
58 Karoo basalts of South Africa and Antarctica.

59 **Falkland Islands Dyke Swarm**

60 Dolerite dykes, mostly of Jurassic age, are widespread in West Falkland and rather sparse in
61 East Falkland (Fig. 2; Greenway 1972; Mussett & Taylor 1994; Thistlewood *et al.* 1997;
62 Mitchell *et al.* 1999; Stone *et al.* 2008, 2009; Richards *et al.* 2013). Distinct sub-swarms of
63 dykes have been recognized based on azimuth of exposed intrusions and aeromagnetic
64 anomalies (Mitchell *et al.* 1999; Stone *et al.* 2009). Prominent dolerite dykes, tens of metres
65 wide and oriented NE-SW, are present in both West and East Falkland and are reversely
66 magnetized. This suite corresponds to the N-S suite of Mitchell *et al.* (1999), and is of Jurassic
67 age (c. 178-190 Ma; Mussett & Taylor 1994; Stone *et al.* 2009) although the older of these ages
68 were generated by the Ar-Ar method on whole-rock samples and have large errors (e.g R1790
69 190 ± 4 Ma; Mussett & Taylor 1994). E-W oriented olivine-dolerite dykes occur locally in the
70 south of West Falkland, and they form part of a larger suite of intrusions that Stone *et al.* (2009)
71 suggest has a partially radial disposition. In addition, Richards *et al.* (2013) noted that there is a
72 suite of about 40, N-S oriented magnetic anomalies, that may represent intrusions, and these
73 occur across the entire Falkland Islands. Exposed examples from Teal Creek and Peat Banks
74 (Fig. 2) yield $^{40}\text{Ar}/^{39}\text{Ar}$ ages in the range 133-138 Ma and these dykes are likely to be members
75 of the Etendeka suite of south-western Africa (Stone *et al.* 2009; Richards *et al.* 2013). During
76 the current study, $^{40}\text{Ar}/^{39}\text{Ar}$ step-heating analysis was carried-out on separated plagioclase

77 feldspar phenocrysts from three samples, but only one of these yielded useful information.
78 Sample WI-5, a NE-SW oriented dyke from Weddell Island (Fig. 2), which is also within the
79 area of the radial swarm identified by Richards *et al.* (2013), contains abundant plagioclase
80 phenocrysts, and yielded a precise age of 182.3 ± 1.5 Ma (Fig. 3). This confirms a Jurassic age
81 for some of the Falkland Islands intrusions, and it is within error of the 178.6 ± 4.9 Ma
82 determined by Stone *et al.* (2008) for an aphyric NE-SW dyke from Port Sussex Creek, East
83 Falkland (Fig. 2).

84 Selected major and trace element abundances *versus* weight % MgO for 139 intrusions from
85 the Falkland Islands, including 109 from this study and 30 from Mitchell *et al.* (1999), are
86 shown in Fig. 4 and representative analyses are given in Table 1. Mitchell *et al.* (1999) divided
87 the intrusions of the Falkland Islands into two main N-S and E-W suites based on azimuth, field
88 occurrence, petrography, mineral chemistry and whole-rock geochemical data. A subsidiary
89 three magma types were also tentatively identified by Mitchell *et al.* (1999), including ‘evolved
90 N-S’, Lively Island and Mount Alice types. The reassessment of the spatial distribution,
91 orientation and age of the dyke swarms by Stone *et al.* (2009) and Richards *et al.* (2013), along
92 with the much enlarged data set for the igneous rocks of the Falkland Islands generated for this
93 study, now allows the identification of five individual geochemical types of intrusions. The
94 criteria used to separate the different groups of intrusions are given in Table 2 and are illustrated
95 in Figs 4 to 9. A description of each suite is given below.

96 ***Port Sussex Creek-type intrusions (PST).*** All the N-S dykes of Mitchell *et al.* (1999) are
97 included in this suite of intrusions, with the exception of the ‘evolved type’ described by
98 Mitchell *et al.* (1999) which will be discussed under the Dyke Island Type (samples NHF17 and
99 NGF15). PST intrusions are widely distributed across both East Falkland and West Falkland, all
100 are sub-vertical with an azimuth of NE-SW, and they are consistently between 8 and 10 m in
101 thickness. A typical example occurs at Port Sussex Creek, East Falkland, (MHF1; Table 1, Fig.
102 2), and is an 8m wide, sub-vertical, medium-grained, spheroidally-weathering dolerite dyke with

103 an azimuth of 45° (NE-SW) and an age of 178.6±4.9 Ma (Stone *et al.* 2008). The texture is
104 equigranular and intersertal. Pyroxene is enstatite (En₇₀Wo₄Fs₂₆), pigeonite (En₅₁Wo₁₃Fs₃₆) and
105 augite (Fig. 5) and the feldspar is labradorite (An₇₀). All PST intrusions contain both augite and
106 pigeonite, with more mafic samples containing orthopyroxene. Olivine (Fo₅₀₋₇₁) is rare in this
107 suite of rocks and is restricted to intrusions with Mg# >58 (e.g. FAR1503 and NGF16; Table 1,
108 Fig. 4). Whole-rock MgO contents vary from 5.9-9.5 wt% (Mg# 50-62) and SiO₂ (53-55wt%) is
109 higher for a given MgO concentration than any of the other Falkland Islands intrusions (Fig. 4).
110 The PST intrusions are characterized by low CaO (8.1-9.8wt%) for a given MgO content
111 compared to other Falkland Islands intrusions. TiO₂ abundances (0.9-1.2wt%) are typical of the
112 low TiO₂ Gondwana break-up related LIPs of the southern hemisphere and distinguishes them
113 from the high TiO₂ (>2.5wt%) suite of break-up related magmas (e.g. Brewer *et al.* 1992).
114 Abundances of Cr are unusually high (up to 648ppm) for samples with SiO₂ in their range, and
115 are reflected in the high Cr content of orthopyroxene. Abundances of Nb and Y are restricted to
116 2-5 and 19-23ppm respectively. PST intrusions are LREE enriched (Fig. 6) with [La/Yb]_N in the
117 range 3.2-3.9 and samples lack any significant Eu anomaly (Eu/Eu* 0.89-0.97). La/Ta and
118 Th/Ta are the highest of any of the Falkland Islands samples analysed (44-52 and 5.9-8.6
119 respectively), and consequently, on ORB-normalized multi-element diagrams (Fig. 7), samples
120 exhibit a marked trough in the abundances of Ta and Nb relative to Th, U, K and La. [Ta/Yb]_N
121 is in the range 2.0 to 2.6, the lowest values for any of the Falkland Islands intrusions. Ti/Zr and
122 P/Zr (55-60 and 4.5-6.3 respectively) are such that all PST intrusions exhibit a minor trough at
123 Ti and P relative to adjacent elements on ORB-normalized diagrams. εNd₁₈₂ varies from -5.5 to -
124 11.0 and is accompanied by radiogenic Sr-isotopic compositions (⁸⁷Sr/⁸⁶Sr₁₈₂ 0.7070-0.7134),
125 although Sr-Nd isotope covariations are rather scattered (Fig. 8). Pb-isotopic compositions form
126 an array that is close to the Geochron (²⁰⁷Pb/²⁰⁴Pb =15.55-15.65), and extends to ²⁰⁶Pb/²⁰⁴Pb
127 ratios of up to 18.40. ²⁰⁷Pb/²⁰⁴Pb exhibits a negative correlation with εNd₁₈₂ for PST intrusions
128 (Fig. 8). Marked negative correlations between 1/Sr and ⁸⁷Sr/⁸⁶Sr₁₈₂, εNd₁₈₂ and Th/Ta and a

129 positive correlation between MgO and ϵNd_{182} (Fig. 9) suggests that PST dykes underwent
130 interaction with a high $^{87}\text{Sr}/^{86}\text{Sr}_{182}$ (> 0.714), low ϵNd_{182} (< -12) component that had $\text{Th}/\text{Ta} > 9$,
131 and that interaction was concomitant with crystallization

132 ***E-W intrusions.*** The E-W samples reported by Mitchell *et al.* (1999) are from a single intrusion,
133 approximately 10m wide, which can be traced for more than 30 km from Fox Bay West to
134 Queen Charlotte Bay (Fig. 2). These samples are generally medium-grained olivine-phyric
135 dolerites (Fo_{82} at 11wt% MgO in the whole-rock), the only pyroxene present being augite (Fig.
136 5). During the current study, intrusions with similar petrographic and mineralogical
137 characteristics were found around South Harbour and on Weddell Island (Fig. 2). E-W
138 intrusions are distinguished from the PST (Fig. 10) by their lower SiO_2 contents (48-52wt%)
139 and higher Ti/Zr (80-95) for a similar range in TiO_2 , and MgO content (1.0-1.4 and 4.8-11.4wt
140 % respectively). E-W intrusions have $[\text{La}/\text{Yb}]_N$ in the range 2.1-4.0 (Fig. 6) and no
141 appreciable Eu anomaly ($\text{Eu}/\text{Eu}^* 0.89$ -1.0). $[\text{Ta}/\text{Yb}]_N$ ratios are in the range 2.8 to 4.7, and all
142 samples exhibit a negative Nb, Ta trough relative to the LILE (La/Ta , 16-27, Th/Ta 2.2-2.8) but
143 this is not as pronounced as that for the PST intrusions (Fig. 7). E-W intrusions have isotopic
144 compositions that are close to, or slightly depleted relative to the Chondritic Uniform Reservoir
145 ($\epsilon\text{Nd}_{182} = -0.4$ to 3.0; $^{87}\text{Sr}/^{86}\text{Sr}_{182} = 0.7036$ -0.7058) and have Pb-isotopic compositions that lie
146 just above the NHRL (Fig. 8).

147 ***Lively Island intrusion.*** A single 30m thick intrusion which is exposed on Lively Island has
148 noticeably lower TiO_2 for a given MgO content than any other of the Falklands Islands
149 intrusions ($\text{TiO}_2 = 0.8\text{wt}\%$ at 6wt% MgO) and the data falls close to the compositional trend for
150 low TiO_2 Ferrar dolerites from the Transantarctic Mountains (Fig. 11). Characteristic
151 mineralogical features are the presence of sparse, Mg-rich biotite and rare Ca-poor groundmass
152 pyroxene (Fig. 5). The intrusion has a LREE-enriched REE profile ($[\text{La}/\text{Yb}]_N = 3.2$; Fig. 6)
153 which lacks a significant negative Eu anomaly ($\text{Eu}/\text{Eu}^* = 0.87$). La/Ta and Th/Ta (20.4 and 3.2
154 respectively) are similar to E-W intrusions and considerably lower than for PST intrusions

155 (Table 2). The Lively Island intrusion contains radiogenic Nd and unradiogenic Sr ($\epsilon\text{Nd}_{182} -0.5$,
156 $^{87}\text{Sr}/^{86}\text{Sr}_{182}$ c. 0.7060) compared to PST intrusions.

157 **Dyke Island Type (DIT).** The greatest concentration of DIT intrusions is on aptly-named Dyke
158 Island (Fig. 2). Sample WI-5 which yielded the Ar-Ar age of 182.3 ± 1.5 Ma which crops out on
159 Weddell Island (Fig. 2) is of this type. In addition, the evolved N-S samples described by
160 Mitchell *et al.* (1999) are of this type (e.g. NHF17; Fig. 2). Intrusions are generally <50 cm
161 thick, they may contain abundant plagioclase \pm augite phenocrysts (samples WI-5, MHF14.9
162 and FAR338; Fig. 5), or more commonly they are medium- to fine-grained aphyric basaltic-
163 andesites and andesites with rare rhyolite sheets occurring locally. DIT intrusions represent an
164 expanded fractionation series with MgO varying from 5.6 to <0.1wt%, over a range of 51-
165 75wt% SiO_2 . Ti/Zr is in the range 32-55 for samples with 4.0-5.6wt% MgO, and for samples
166 with <1wt% MgO, Ti/Zr falls to <5 (Fig. 4). All DIT intrusions have higher concentrations of
167 the incompatible elements Zr, Nb and Y than any of the other intrusions from the Falkland
168 Islands, and exhibit strong positive linear correlations between these elements. On a plot of TiO_2
169 *versus* MgO (Figs 4 & 11) DIT intrusions can be divided into three distinct series; i) a low TiO_2
170 series which forms and extension of the data array for PST intrusions; ii) a high TiO_2 series with
171 MgO in the range 2.5-4.0wt% MgO with $\text{TiO}_2 > 1.7\text{wt}\%$; and iii) acid intrusions with <2wt%
172 MgO.

173 DIT intrusions are LREE-enriched ($[\text{La}/\text{Yb}]_N = 4.1-6.6$; Fig. 6) and exhibit stepwise
174 increases in both LREE and HREE abundances with decreasing MgO with the most evolved
175 sample (MHF41.3, 0.06wt% MgO) having $\text{La}_N = 190$ and $\text{Yb}_N = 44$. The development of a
176 progressively larger negative Eu anomaly ($\text{Eu}/\text{Eu}^* = 0.85-0.71$) with decreasing MgO, attests to
177 the importance of plagioclase fractionation during their petrogenesis. Th/Ta and La/Ta for the
178 DIT intrusions (2.4-3.4 and 17-26 respectively) are similar to those for the E-W intrusions.
179 Multi-element diagrams (Fig. 7) show that DIT intrusions exhibit troughs at Ti and P relative to
180 adjacent elements, and a progressively larger negative Sr anomaly is developed with decreasing

181 MgO. Plagioclase-phyric samples WI-5 and FAR338 exhibit a positive Sr spike in Fig. 7, which
182 is presumably a result of accumulation of plagioclase feldspar, although neither sample exhibits
183 a Eu anomaly. The distribution of trace elements in DIT intrusions bears a strong resemblance to
184 those for Ferrar dolerites from the Transantarctic Mountains (Fig. 7). DIT intrusions have
185 $^{87}\text{Sr}/^{86}\text{Sr}_{182}$ in the range 0.7055-0.7170 but all samples with $^{87}\text{Sr}/^{86}\text{Sr}_{182} > 0.7090$ contain < 2
186 weight % MgO. ϵNd_{182} falls in the range -2.8 to +0.6, and there is no systematic variation
187 between MgO, ϵNd_{182} or $^{87}\text{Sr}/^{86}\text{Sr}_{182}$ (Figs 8 & 9).

188 **Mount Alice Type intrusions (MAT).** MAT intrusions are restricted to the south-western area of
189 West Falkland, around South Harbour, Dyke Island and Cape Orford (Fig.1) and are early
190 Jurassic in age (188 ± 2 Ma for sample MA3; Mussett & Taylor 1994). MAT intrusions are
191 generally <1 m thick and are characterized by plagioclase \pm augite \pm olivine phenocrysts in a
192 fine-grained groundmass. Since the area in which the MAT intrusions occur is within the region
193 of the radial dyke swarm described Richards *et al.* (2013), azimuths cannot be used as one of
194 their classification criteria, although in the region of Cape Orford, MAT dykes are generally
195 oriented E-W (Mussett & Taylor 1994; Thistlewood *et al.* 1997). A typical example (MFH15.2)
196 contains sparse, scattered phenocrysts of olivine (Fo_{80}), calcic augite ($\text{En}_{31}\text{Fs}_{25}\text{Wo}_{44}$; Fig. 5) and
197 labradorite (An_{60}). MgO varies from 6-12wt%, and the MAT intrusions have the lowest SiO_2
198 (46-50wt%) for a given MgO content of any of the Falklands Islands samples (Fig. 4). TiO_2
199 abundances (1.3-2.0wt%) overlap with those for both the PST and E-W intrusions but Ti/Zr is in
200 the range 90-150 (Fig. 10) which is considerably higher than any other of the Falkland Islands
201 intrusions. MAT intrusions have $[\text{La}/\text{Yb}]_{\text{N}}$ in the range 1.8-3.1 (Fig. 6) and flat to slightly
202 LREE-depleted REE profiles for elements La to Sm ($[\text{La}/\text{Sm}]_{\text{N}}$ 0.9-1.5). On multi-element
203 diagrams (Fig. 7), MAT intrusions exhibit a positive Sr spike relative to N-ORB, but otherwise
204 have smooth profiles from elements Nd to Lu, with Ti/Zr and P/Zr (98-130 and 8.0-10.4
205 respectively) in the range for normal ORB (Ti/Zr c. 100, P/Zr c. 6.9; Sun & McDonough 1987).
206 Unlike all the other Falkland Islands intrusions, the MAT have Th/Ta and La/Ta (0.7-1.0 and

207 13-17 respectively) which are also within the range for normal ocean ridge basalts and
208 asthenosphere-derived basalts (Sun & McDonough 1987). Sr- & Nd-isotopic compositions fall
209 in the upper-left quadrant of Fig. 8, with $\epsilon\text{Nd}_{182} > 5$ and $^{87}\text{Sr}/^{86}\text{Sr}_{182} < 0.7040$. Pb-isotopic
210 compositions fall just above the NHRL with $^{206}\text{Pb}/^{204}\text{Pb}$ in the range 18.2-18.5 (Fig. 8).

211 **Petrogenesis of the Falkland Islands intrusions**

212 The diversity of major and trace element geochemistry and isotopic compositions of the
213 Falkland Islands intrusions requires an equally diverse range of petrogenetic histories. In
214 particular, the observed ranges of isotopic compositions described above are likely to require
215 variable interaction between isotopically depleted melts from mantle peridotite with melts
216 derived from continental lithosphere, which in some cases, must of considerable antiquity.
217 Consequently, before attempting to make regional comparisons between the Falkland Islands
218 intrusions and other Gondwana break-up related low TiO_2 suites within the southern
219 hemisphere, an assessment of the petrogenetic history of each of the suites of Falkland Island
220 intrusions will be made in turn below.

221 ***PST intrusions***

222 PST and low TiO_2 DIT intrusions exhibit variations in major element compositions that fall
223 along the same fractionation trend as low TiO_2 basaltic-andesites and andesites from the Theron
224 Mountains (Fig. 11). However, PST and DIT intrusions cannot be related to one another by
225 simple crystal fractionation because their Sr-, Nd- and Pb-isotopic compositions differ
226 significantly from one another (Fig. 8). The high $^{87}\text{Sr}/^{86}\text{Sr}_{182}$ (> 0.710) and unradiogenic Nd-
227 isotopic compositions of the PST is a feature they share with Ferrar Province igneous rocks.
228 Fleming *et al.* (1995) and Molzhan *et al.* (1999) demonstrated that elevated $^{87}\text{Sr}/^{86}\text{Sr}_{182}$ (0.7090-
229 0.7112) of MFCT basalts was partly a function of Rb and Sr mobility during a Cretaceous (97-
230 125 Ma) hydrothermal event. However, the observed range in ϵNd_{182} in the same samples (-4.8
231 to -5.6) is unlikely to be the result of alteration, and Fleming *et al.* (1995) concluded from

232 analysis of phenocryst phases, that prior to alteration, MFCT basalts must have had
233 $^{87}\text{Sr}/^{86}\text{Sr}_{182} \geq 0.7090$. Alteration by the same regional hydrothermal thermal event cannot be used
234 as an explanation for variability in the Sr-isotopic compositions of PST intrusions because the
235 Falkland Islands would have already broken-away from the Antarctic continent by this time. In
236 addition, the range of ϵNd_{182} from -6 to -12 over the limited range of $^{87}\text{Sr}/^{86}\text{Sr}_{182} = 0.7110$ -
237 0.7115 , for the PST intrusions, requires potential contaminants that had a range of Nd-isotopic
238 compositions and were therefore probably of differing ages.

239 **Interaction with the continental lithosphere.** For the PST intrusions, the variations shown in
240 Fig. 9 indicate that Sr- and Nd-isotopic variations were imposed on the magmas concomitant
241 with fractional crystallization, by assimilation with fractional crystallization (AFC) or a similar
242 process. The relationships shown in Fig. 9 require that Sr behaved incompatibly during
243 fractional crystallization of the PST suite. The crystal cumulate formed during AFC cannot,
244 therefore, have been plagioclase-rich. To generate the range of Sr-isotopic compositions seen in
245 the PST intrusions requires a source with $^{87}\text{Sr}/^{86}\text{Sr}_{182} \leq 0.7075$, and contaminants with
246 $^{87}\text{Sr}/^{86}\text{Sr}_{182} > 0.7130$ and a range of ϵNd_{182} , which must be ≤ -6.0 for all samples. Least-squares
247 modelling of the extract and evolved liquid from a starting composition with 9.6wt% MgO
248 (NGF16) to evolved composition with 6.78wt% MgO (MHF5.1; Table 3) requires 21%
249 crystallization of an assemblage of orthopyroxene (74.7%), plagioclase (18.9%) and minor
250 augite (6.4%). With only 18.9% of the fractionating assemblage being plagioclase, D_{Sr} would
251 have been < 1 which is consistent with the relationship between $1/\text{Sr}$ and $^{87}\text{Sr}/^{86}\text{Sr}_{182}$ in Fig. 9.
252 In addition, Demarchi *et al.* (2001) showed that orthopyroxene is on the liquidus of Ferrar
253 tholeiites at 1.0-1.5 GPa, suggesting that magmatic differentiation of the PST intrusions
254 occurred at depths ≥ 30 km.

255 Sr- and Nd-isotopic compositions for PST intrusions fall in an intermediate position between
256 the data for CT1 basalts of Dronning Maud Land and the Karoo (Fig. 12). Luttinen & Furnes
257 (2000) argued that the extreme Nd-isotopic compositions ($\epsilon\text{Nd}_{182} \leq -17$) of CT1 basalts were the

258 result of interaction between a mantle-derived magma and Archean (3.0 Ga) Grunehogna
259 cratonic lithosphere (Fig. 1). Riley *et al.* (2006) used AFC and energy-constrained recharge
260 AFC to model the isotopic compositions of Karoo basaltic rocks using an ORB-like source and
261 an assimilant with $\epsilon\text{Nd}_{182} = -4$ and $^{87}\text{Sr}/^{86}\text{Sr}_{182} = 0.710$, and showed that the observed isotopic
262 variability in the basalts could be explained partly by these processes. In Fig. 12 three AFC
263 trajectories are plotted and the parameters used to generate the curves are given in Table 4.
264 These are not designed to fully explain the isotopic diversity in Gondwana low TiO_2 continental
265 flood basalts, they have been generated in an attempt to constrain possible and impossible
266 petrogenetic processes. The starting composition has been kept constant, and is based on that of
267 largely uncontaminated low TiO_2 basalts with $\epsilon\text{Nd}_{182} = 2$ and $^{87}\text{Sr}/^{86}\text{Sr}_{182} = 0.7035$. For all three
268 modelled AFC trends, the ratio of the country rock assimilated to crystal cumulate formed, R ,
269 has been set at 0.40, a value that is appropriate for crystallization in the middle- to upper-crust
270 (Riley *et al.* 2006; Hole *et al.* 2015). D_{Sr} and D_{Nd} are set at 0.5 and 0.1 respectively, to simulate a
271 cumulate with approximately 25% plagioclase, and 75% ferromagnesian minerals. This means
272 that all three AFC trajectories approach the composition of the most contaminated magma for \leq
273 20% AFC (Table 4). Increasing the value of R to 0.5 for any of the models does not significantly
274 change the shape of the trajectories, but decreases the amount of AFC that is needed to reach the
275 target compositions to $\leq 12\%$, and conversely, decreasing R to 0.3 requires $\leq 25\%$ AFC. For the
276 CT1 AFC model, the contaminant represents 3.0 Ga Grunehogna Craton (Fig. 1) felsic granulite,
277 with $\epsilon\text{Nd}_{182} = -50$ and $^{87}\text{Sr}/^{86}\text{Sr}_{182} = 0.712$ (felsic xenolith sample X4-AVL of Luttinen & Furnes
278 2000). The PST-1, mixing line intersects the lowest ϵNd_{182} samples in the PST suite, and the
279 contaminant represents a 2.2 Ga Palaeoproterozoic felsic granulite with $\epsilon\text{Nd}_{182} = -20$ and
280 $^{87}\text{Sr}/^{86}\text{Sr}_{182} = 0.720$ (Luttinen & Furnes 2000). The PST-2 mixing line, which also intersects the
281 majority of data for Karoo basalts and lowest $^{87}\text{Sr}/^{86}\text{Sr}_{182}$ (~ 0.7090) samples of Ferrar igneous
282 rocks, representing mixing between a mantle-derived magma and 1.0-1.5 Ga felsic crust with
283 $\epsilon\text{Nd}_{182} = -10$ and is the same contaminant as that suggested by Riley *et al.* (2006) for Karoo

284 basalts. Plate reconstructions place the Falkland Islands mainly within the 1.0-1.5 Ga
285 Namaqualand-Natal-Maudheim-Mozambique belt (Thistlewood *et al.* 1997) and on the
286 continuation of the Cape Fold Belt (Fig. 1). Mesoproterozoic crust is therefore a likely candidate
287 for basement to the Falkland Islands, although there are no isotopic data for the Cape Meredith
288 metamorphic complex. What is also clear is that cratonic basement like that involved in the
289 petrogenesis of the CT1 basalts affected neither the PST intrusions nor Karoo low TiO₂ basaltic
290 rocks. AFC models with geologically reasonable parameters and appropriate ages of potential
291 basement contaminants can therefore produce the observed variations in the Sr- and Nd-isotopic
292 characteristics of the PST intrusions for <20% AFC.

293 **Pyroxenite versus peridotite sources.** PST intrusions with MgO > 8 weight % have lower CaO
294 abundances (c. 8.5 weight %) than any other of the other Falkland Islands intrusions (Figs. 4 and
295 13). Such compositions are uncommon in continental flood basalts provinces. Orthopyroxene
296 was the dominant fractionating phase during crystallization of the PST (Table 3) and estimates
297 of more primitive compositions can be calculated by incrementally adding enstatite to a mafic
298 PST composition. Addition of 30% enstatite to sample NGF16 yields magma with ~15wt%
299 MgO and ~7.5wt% CaO. Compositions such as these are also found in the CT1 basalts of
300 Dronning Maud Land (Fig. 13a). An unusual feature of the PST intrusions is their Si-
301 oversaturated nature and high Cr content (Fig. 13b) which is also reflected in unusually high Cr
302 content of component orthopyroxene (e.g. enstatite in MHF3.2 has 0.74wt% Cr₂O₃ at
303 MgO/FeO = 2.8). In terms of major element compositions, PST intrusions bear strong
304 similarities with magnesian andesite from continental subduction settings (e.g. Baker *et al.*
305 1994; Sato *et al.* 2014). For example, high-Mg andesites from Mt Shasta have a similar range of
306 MgO to PST intrusions (Fig. 13a) which is accompanied by SiO₂ = 51.5-54.0wt%, Cr = 245-695
307 ppm, Ni =99-235 ppm, TiO₂ = 0.6-0.8wt% and CaO =8.6-9.6wt%. One mechanism that has
308 been suggested for the production of high-Mg andesite is the interaction of slab-derived adakitic
309 melts with mantle peridotite during subduction (Heinonen *et al.* 2014). A link to the previous

310 subduction history of the mantle source from which Ferrar and Karoo basaltic rocks were
311 derived has been made by a number of workers (e.g. Brewer *et al.* 1992; Storey *et al.* 1992;
312 Heinonen *et al.* 2014) and in particular, the characteristic trough at Nb and Ta relative to
313 adjacent elements (Fig. 7) has been interpreted as an inherited subduction signature.

314 Herzberg & Asimow (2008) note that primary magmas derived from the melting of
315 pyroxenite will exhibit relative CaO depletion compared to melts from a peridotite source
316 because of the dominance of residual clinopyroxene in the source region during partial melting
317 of pyroxenite. Given the position that data for the PST occupy in Fig. 12, it seems clear that
318 their major element compositions are not consistent with an origin by melting of mantle
319 peridotite. It is well established that pyroxenite can be formed at the base of the lithosphere as a
320 result of accumulation of mafic phases during basaltic magmatism (e.g. Downes *et al.* 2007).
321 Such accumulative pyroxenite can yield magma by partial melting at some later stage, promoted
322 by a new phase of mafic magmatism and by interaction with peridotite-derived melts (Lambart
323 *et al.* 2013). The generation of silica-enriched pyroxenite melts is possible, which can yield Si-
324 oversaturated melts like those of the PST intrusions (Lambart *et al.* 2013). It is therefore
325 suggested that the PST were derived from a pyroxenite-rich source that was emplaced at the
326 base of the lithosphere during the prolonged subduction history of Gondwana. Metasomatism of
327 the pyroxenite by slab-derived fluids and melt, imparted a subduction signature to the
328 pyroxenite. When subjected to the high mantle potential temperatures associated with the mantle
329 plume beneath Dronning Maud Land at c. 180 Ma (T_P up to 1600°C; Heinonen *et al.* 2010), the
330 pyroxenite underwent partial melting and produced the primary melt precursor to the PST
331 intrusions. These melts then interacted with fusible, felsic continental crust to produce the
332 geochemical composition of the more evolved PST compositions by AFC, or a related process.
333 Extrapolation of the MgO - ϵNd_{182} trend for the PST to higher MgO contents (Fig. 9a), suggests
334 that a primitive composition with 15 weight % MgO might have had $\epsilon Nd_{182} \sim 0$, and the

335 correlation between $1/\text{Sr}$ and Sr-isotopic compositions requires the source to have $^{87}\text{Sr}/^{86}\text{Sr}_{182} \leq$
336 0.7075.

337 ***E-W intrusions***

338 Least-squares modelling of the extract and evolved liquid from a starting composition ECF12 to
339 more evolved sample ECF44 (Table 3) requires crystal fractionation of 57% olivine and 40%
340 plagioclase feldspar with little contribution from augite (c. 2.6 %) which is a typical
341 crystallizing assemblage for tholeiitic melts at pressures ≤ 0.5 GPa (e.g. Hole & Morrison 1992;
342 Villiger *et al.* (2007), requiring E-W intrusions to have last equilibrated at $< \sim 15$ km depth,
343 within the crust. This is in contrast to the > 1.0 GPa equilibration required by PST intrusions.
344 The isotopic compositions of E-W intrusions require derivation from a depleted mantle source
345 (Figs 8), but they have higher Th/Ta (2.2-2.8) and La/Ta (16.4-26.1) than would be expected if
346 they were derived from asthenospheric mantle (Th/Ta ~ 1.0 and La/Ta ≤ 18 ; Sun & McDonough
347 1989) and they also exhibit a noticeable trough at Nb and Ta relative to adjacent elements in
348 Fig. 7, a feature that is most often attributed to interaction with continental lithosphere.
349 However, the extent of this interaction must either have been limited, or the source from which
350 the E-W intrusions were derived had a Th/Ta > 2.0 and La/Ta > 26 . The low pressure
351 equilibration of E-W intrusions, coupled with their depleted isotopic compositions may suggest
352 that they were emplaced during a period of crustal attenuation and were thus able to escape
353 interaction with continental lithosphere.

354 ***DIT and Lively Island intrusions***

355 In contrast to the PST intrusions, the sub-horizontal arrays delineated by DIT intrusions in Fig.
356 9a, suggests that AFC or a similar process was not important during their petrogenesis.
357 However, a negative correlation between Th/Ta and ϵNd_{182} for the DIT intrusions (Fig. 9b) may
358 require minor modification by a crustal component with Th/Ta ≥ 3.0 . A characteristic feature of
359 the DIT samples is that they have ϵNd_{182} in range -2.8 to +0.6, but with only a single analysed
360 sample (NHF17) having $\epsilon\text{Nd}_{182} < -1$. In addition, the Lively Island dyke, which falls close to the

361 fractionation trend for the MFCT basaltic rocks of the Transantarctic Mountains (Fig. 11), has
362 Sr- and Nd-isotopic compositions ($^{87}\text{Sr}/^{86}\text{Sr}_{182}$ c. 0.7052, $\epsilon\text{Nd}_{182} = -0.5$ to -1.4) that do not
363 require the significant isotopic enrichment seen in the Ferrar dolerites (ϵNd_{182} in the range -3.3
364 to -5.3 ; Fleming *et al.* 1995; Hergt *et al.* 1989). The source of the low TiO_2 DIT magmas could,
365 therefore, have had $\epsilon\text{Nd}_{182} > 0$, $^{87}\text{Sr}/^{86}\text{Sr}_{182} < 0.7050$, $\text{Th}/\text{Ta} < 2.5$ and $\text{La}/\text{Ta} < 20$.

366 ***MAT intrusions***

367 The positive ϵNd_{182} (2.7-3.6) and low Th/Ta , La/Ta and $[\text{La}/\text{Yb}]_N$ (0.8-1.0; 12.8-17.3 and 1.9-
368 3.7 respectively) of MAT intrusions suggests that they were derived from an asthenospheric
369 source, and escaped significant interaction with lithosphere. The most satisfactory explanation
370 for the geochemical compositions of these rocks is that they were generated by decompression
371 melting of the asthenosphere during the rifting stage of Gondwana break-up. In this respect they
372 have similar geochemical compositions to the ORB-like Rooi Rand basaltic dykes of the
373 southern Lebombo (Cox & Bristow 1984, which post-date the main magmatic phases in the
374 region by about 5 Myr (Jourdan *et al.* 2007).

375 ***Cretaceous intrusions***

376 Until more data are forthcoming, the origin and affinity of the Cretaceous Teal Creek intrusion
377 reported by Stone *et al.* (2009) remains somewhat obscure. Major element data for the intrusion
378 plot close to the Theron Mountains low TiO_2 trend in Fig. 6, but the intrusion has higher Fe_2O_3
379 (c. 15.9wt%) at 5.7wt% MgO than any of the data for the intrusions presented here. What is
380 clear, is that there is an extensive suite of low TiO_2 basalts within the Etendeka Province (e.g.
381 Gibson *et al.* 2005; Thompson *et al.* 2001) from which it could be related. However, none of the
382 groups of intrusions described here carries a similar signature to that presented by Stone *et al.*
383 (2009) for the Teal Creak dyke.

384 **Provinciality and chemical affinities of Falkland Islands intrusions**

385 A number of authors have noted that there are spatially constrained variations in major and
386 trace element compositions within the Jurassic Gondwana break-up related flood basalts
387 provinces of the Southern Hemisphere (e.g. Brewer *et al.* 1992; Luttinen & Furnes 2000; Riley
388 *et al.* 2006). Figs 11 and 14 illustrate the variability in abundances of MgO, TiO₂, SiO₂ and
389 Ti/Zr for Falkland Island intrusions, along with igneous rocks which are defined as being either
390 Karoo or Ferrar magma types, or those which are considered to be transitional between the two
391 magma types (Brewer *et al.* 1992; Luttinen & Furnes 2000; Riley *et al.* 2006). In the following
392 sections, we will examine the geochemical affinities of the Falklands Islands intrusions in
393 relationship to other early Jurassic flood basalts of Gondwana.

394 ***PST intrusions***

395 PST intrusions exhibit strong similarities to CT1 basalts of Dronning Maud Land (e.g. Fig. 14),
396 and show some overlap with the compositional field for samples from the Theron Mountains
397 and Transantarctic Mountains. In terms of incompatible trace elements, PST dykes exhibit
398 almost identical multi-elements patterns to sample SA.6.1 (Fig. 7; Riley *et al.* 2006) from
399 KwaZulu-Natal, with which they share also unradiogenic Nd-isotopic compositions (e.g. SA.6.1
400 $\epsilon_{\text{Nd}_{182}} = -8.9$). Within the CT1 basalts of Dronning Maud Land, very similar compositions to
401 PST intrusions can be found (e.g. B70-AVL; Luttinen & Furnes 2000) again with many basalts
402 in the CT1 suite having unradiogenic Nd-isotopic compositions (Fig. 12). Furthermore, both
403 CT1 and PST magmas required derivation from a pyroxenite-rich, CaO deficient, source region
404 (Fig. 13). It is with some confidence that we conclude that the PST, CT1 and some KwaZulu-
405 Natal basalts were derived from very similar source regions, had similar petrogenetic histories
406 and represent the same phase of pre-break-up magmatism.

407 ***E-W intrusions***

408 These igneous rocks exhibit a strong geochemical affinity with basalts from Kirwanveggan
409 (Harris *et al.* 1990) and Schirmaker Oasis (Sushchevskaya *et al.* 2009), Dronning Maud Land
410 (Figs 11 and 14). A notable characteristic of all the above samples is that they have radiogenic

411 Nd-isotopic compositions ($\epsilon\text{Nd}_{182} = 2-6$) $^{87}\text{Sr}/^{86}\text{Sr}_{182}$ in the restricted range 0.7040-0.7060 and
412 $^{206}\text{Pb}/^{204}\text{Pb}$ in the range 17.97-18.49 and plot close to the NHRL in Fig. 8. These isotopic
413 characteristics, coupled with $\text{Ti}/\text{Zr} = 70-90$ and $\text{SiO}_2 = 47.0-52.8\text{wt}\%$, clearly separates
414 Kirwanveggan, Schirmaker Oasis and Falkand Islands E-W intrusions from PST intrusions. E-
415 W intrusions also fall within the compositional field for basalts from the Central Karoo of South
416 Africa in Fig. 14, and intrusions with compositions similar to those of Falkland Islands E-W
417 intrusions are prevalent in the Golden Valley Sill Complex (Neumann *et al.* 2011).

418 ***DIT and Lively Island intrusions***

419 In Fig. 14b, DIT intrusions exhibit almost complete overlap with the MFCT Ferrar dolerites of
420 the Transantarctic Mountains. However, consideration of Fig. 11, shows that DIT intrusions are
421 not of the same low TiO_2 (<0.5-1.2wt%) lineage of the MFCT. However, DIT intrusions do
422 have compositions that overlap with those for low TiO_2 Theron Mountains basalts and samples
423 from KwaZulul-Natal that Riley *et al.* (2006) and Brewer *et al.* (1992) argued were transitional
424 between Ferrar and Karoo magma types. We concur with this hypothesis, and given the position
425 that the Falkland Islands occupied in southern Gondwana at the time of Karoo and Ferrar
426 magmatism, this seems entirely reasonable.

427 The Lively Island intrusion is the only member of the intrusive suite of rocks of the Falkland
428 Islands that falls within the compositional range for MFCT samples from the Transantarctic
429 Mountains in Figs 11 and 14. However, the Lively Island intrusion has considerably lower
430 La/Ta and Th/Ta (20.5 and 3.2 respectively) than the majority of the MFCT dolerites (La/Ta 19-
431 47; Th/Ta 4.3-23.3), and the Lively Island dyke also has considerably more radiogenic Nd
432 ($\epsilon\text{Nd}_{182} = -0.5$ to -1.4) than MCFT dolerites ($\epsilon\text{Nd}_{182} = -4.7$ to -5.7). It is important to note, that
433 the Lively Island intrusion is a single body of igneous rock around 30m thick, and consequently
434 is not a volumetrically significant part of the Falkland Islands dyke swarm.

435 ***MAT intrusions***

436 Ti/Zr>90 coupled with SiO₂ of 45.7-51.0wt% are characteristics that MAT intrusions share
437 with CT2 and CT3 basalts from Dronning Maud Land and samples from the Rooi Rand dyke
438 swarm of the southern Lebombo area of southern Africa (Cox & Bristow 1984).. The
439 unradiogenic Sr-isotopic compositions (⁸⁷Sr/⁸⁶Sr₁₈₂ c. 0.7040) and radiogenic Nd-isotopic
440 compositions (εNd₁₈₂ = 2.5-4.0) of E-W intrusions also characterize Rooi Rand and CT2 and
441 CT3 basalts, although the Dronning Maud Land samples have a rather more extended range of
442 isotopic compositions, which Luttinen & Furnes (2000) attribute to conservative amounts of
443 interaction with upper-crustal felsic contaminants.

444 **Mantle potential temperature, rifting and magmatism**

445 Fig. 15a summarizes the available data for olivine equilibration temperatures (T_{OL}) for MAT
446 and E-W basalts and picrites from Dronning Maud. MAT and E-W basalts yield olivine
447 equilibration temperatures of 1245°C and 1330°C respectively, using the method of Putirka *et*
448 *al.* (2007), whilst olivine in picrites from Dronning Maud Land yield T_{OL} up to 1450°C.
449 Converting equilibration temperatures to T_P is problematical if the pressure and extent of
450 melting cannot be independently determined (Herzberg & Asomow 2008; Herzberg & Gazel
451 2009; Hole 2015), which they cannot for the MAT and E-W samples. However, since olivine
452 equilibration temperature increases with increasing pressure of crystallization, synthetic olivine
453 liquids can be calculated for any given temperature and pressure (Herzberg & Gazel 2009). Fig.
454 15b shows the inferred temperature-pressure conditions at which fractional melting terminated
455 for calculated primary magmas from Dronning Maud Land, the Karoo Province of southern
456 Africa, Ferrar dolerites of Antarctica. (Hole 2015). In Fig. 15c, data for basalts from the
457 Cretaceous Etendeka Province of SW Africa (Kieding *et al.* 2011) are given, for which
458 estimates of T_{OL}, estimates of T_P from melt inclusions in ultra-magnesian olivine, and estimates
459 of T_P from the PRIMEL2 model of Herzberg & Asimow (2008) have all been calculated on the
460 same samples. Using the Herzberg & Asimow (2008) model yields T_P = 1500-1550°C and final
461 pressures of melting (P_f) between 1.5 and 4.0 GPa (Fig. 13c). T_P from melt inclusions is 1300-

462 1520°C, whilst T_{OL} is in the range 1250-1400°C and there is an empirical relationship between
463 T_{OL} and melt inclusion T_P which approximates to $T_P = 1.443 \times T_{OL} - 501$ for the Etendeka plume
464 system (Fig. 15). Therefore it seems that within a single plume system, basalts may be
465 generated over ranges of T_P that are larger than the $\pm 50^\circ\text{C}$ error inherent in the calculation
466 methods (Herzberg & Asimow 2009; Hole 2015). Direct application of this empirical
467 observation to the Dronning Maud Land picrites suggest maximum $T_P \sim 1550^\circ\text{C}$, a temperature
468 that is considered to be associated with ‘hot’ mantle plumes such as Iceland at 60 Ma (Fig. 15;
469 Herzberg & Gazel 2009). For Falkland Islands E-W basalts, $T_{OL} \sim 1330^\circ\text{C}$, which implies
470 $T_P \sim 1400^\circ\text{C}$ and for olivine-phyric MAT basalts, $T_{OL} \sim 1250^\circ\text{C}$ implying $T_P \sim 1300^\circ\text{C}$. These T_P
471 estimates for the Falkland Islands E-W and MAT basalts may therefore be reconciled with a
472 model involving melting of mantle with near-ambient temperature ($T_P \geq 1350^\circ\text{C}$), but would
473 require intersection of the dry peridotite solidus at ~ 2.1 GPa (~ 70 km) and all melting to take
474 place in the spinel stability field of the mantle; the most mafic MAT and E-W intrusions have
475 $[\text{La}/\text{Yb}]_N < 2.0$ which does not preclude such an origin. Additionally, near-ambient T_P melting
476 would require the continental lithosphere to be thinned substantially and perhaps to < 50 km, to
477 allow decompression melting to take place. The depleted isotopic compositions of the E-W and
478 MAT intrusions, along with the < 0.5 GPa equilibration of the E-W magmas, provides additional
479 evidence to suggest that these intrusions were emplaced during a period of crustal stretching,
480 possible coeval with the initiation of Gondwana. Nevertheless, whilst there is no primary
481 evidence to suggest T_P was $> 1450^\circ\text{C}$ beneath the Falkland Islands at 180 Ma, it is possible that
482 high-MgO large melt fractions requiring substantially higher T_P exist in the region, but have not
483 been sampled, remains a possibility.

484 The diversity of magma types found in the Falkland Islands, and the position in Gondwana
485 which the islands occupied during magmatism (Fig. 1) is entirely consistent with their being
486 close to the focus of magmatism during continental break-up. We concur with Brewer *et al.*
487 (1992) and Riley *et al.* (2006) that there is considerable overlap in the geographical distribution

488 of the Ferrar and Karoo LIPs, which is most obvious in the Theron Mountains and Falkland
489 Islands. It is also clear, that despite the wealth of geochemical data available for the
490 Transantarctic Mountains and Tasmania, there is no evidence to suggest that volcanic rocks with
491 affinities to the Karoo LIP occur in those areas. With the exception of the ORB-like basalts of
492 the Rooi Rand dyke swarm (Marsh *et al.* 1997; Mitchell *et al.* 1999) which are likely to
493 represent syn-break-up magmas, basaltic rocks with Karoo-type geochemical compositions only
494 extend as far south as the overlap zone in the Theron Mountains.

495 **Conclusions**

496 The Jurassic (c. 182 Ma) intrusions of the Falkland Islands exhibit a broad range of geochemical
497 compositions and at least four main petrogenetic lineages are recognized. PST intrusions were
498 derived by melting of an isotopically-enriched pyroxenite-rich source, followed by
499 orthopyroxene-dominated crystal fractionation at ≥ 1 GPa. Pyroxenite-derived PST magmas
500 subsequently interacted with 'old' (≥ 2.2 Ga) fusible continental lithospheric components by
501 AFC or a related process. The geochemical compositions of DIT intrusions bear striking
502 similarities to igneous rocks of Kwazulu-Natal and the Theron Mountains, which are considered
503 to be transitional in composition between those of the Ferrar and Karoo magma types. A
504 significant number of mafic (Mg# 50-62) E-W and MAT intrusions possess radiogenic Nd- and
505 unradiogenic Sr-isotopic compositions ($^{87}\text{Sr}/^{86}\text{Sr}_{182} < 0.7050$ and $\epsilon\text{Nd}_{182} > 2.5$), also have Th/Ta
506 and La/Ta (< 3.0 and < 25 respectively) that require little input from the continental lithosphere.
507 In addition, E-W intrusions carry mineralogical and chemical fingerprints of equilibration at $<$
508 0.5 GPa. E-W and MAT basalts were probably emplaced during rifting and continental break-up
509 and are likened to the Rooi Rand dykes of the Southern Lebombo of Africa. However, there is
510 currently no evidence to suggest that the Falkland Islands intrusions were derived by melting
511 above a significant mantle thermal anomaly. Early Jurassic plate reconstructions place the
512 Falkland Islands close to the Weddell Triple Junction, perhaps explaining the diversity of
513 igneous rock compositions found in a relatively limited geographical region.

514 **Acknowledgements.**

515 An earlier version of the manuscript was improved by thoughtful comments from two
516 anonymous reviewers. Dr D. Aldis, Falkland Islands Geological Survey, is thanked for
517 providing some samples from Fox Bay West for this study.

518

519 **References Cited.**

- 520 Antonini, P., Piccirillo, E.M., Petrini, R., Civetta, M., D'Antonio, M. & Orsi, G. 1999. Enriched
521 mantle Dupal signature in the genesis of the Jurassic Ferrar tholeiites from the Prince Albert
522 Mountains, (Victoria Land, Antarctica). *Contributions to Mineralogy and Petrology*, **136**, 1-
523 19.
- 524 Baker, M.B., Grove, T.L. and Price, R.C. 1994. Primitive basalts and andesites from the Mt.
525 Shasta region, N. California: products of varying melt fraction and water content.
526 *Contributions to Mineralogy and Petrology*, **118**, 111-129.
- 527 Brewer, T. S., Hergt, J. M., Hawkesworth, C. J., Rex D. C. & Storey B. C. 1992. Coats Land
528 dolerites and the generation of Antarctic continental flood basalts. *In: Storey, B. C.,*
529 *Alabaster, T. & Pankhurst, R. J. (eds) Magmatism and the causes of Continental Break-Up*
530 *Geological Society, London, Special Publications*, **64**, 185-208.
- 531 Burgess, S.D., Bowring, S.A., Fleming, T.H. & Elliot, D.H. 2015. High-precision
532 geochronology links the Ferrar large igneous province with early-Jurassic ocean anoxia and
533 biotic crisis. *Earth and Planetary Science Letters*, **415**, 90-99.
- 534 Coltice, N., Bertrand, H., Rey, P.M., Jourdan, F., Phillips, B.R. & Ricard, Y. 2009. Global
535 warming of the mantle beneath continents back to the Archaean. *Gondwana Research*, **15**,
536 254-266.
- 537 Cox, K.G. & Bristow, J.W. 1984. The Sabine River Basalt Formation of the Lebombo
538 Monocline and south-east Zimbabwe. *In: Petrogenesis of the volcanic rocks of the Karoo*
539 *province*, A.J. Erlank (ed). Special Publication of the Geological Society of South Africa, **13**,
540 124-147.
- 541 Demarchi, G., Antonini, P., Piccirillo, E.M., Orsi, G., Civetta, L. & D'Antonini, M. 2001.
542 Significance of orthopyroxene and major element constraints on the petrogenesis of Ferrar
543 tholeiites from southern Prince Albert Mountains, Victoria Land, Antarctica. *Contributions to*
544 *Mineralogy and Petrology*, **142**, 127-146.
- 545 Downes, H., Upton, B.G.J., Connolly, J., Beard, A.D. & Bodinier, J-L 2007. Evidence for late
546 Palaeozoic crustal underplating beneath SW Scotland Petrology and geochemistry of a
547 cumulate xenolith suite from Bute. *Journal of the Geological Society, London*, **164**, 1217-
548 1231.
- 549 Elliot, D.H. 2013. The geological and tectonic evolution of the Transantarctic Mountains: a
550 review. *In: Hambrey, M.J., Barker, P.F., Barrett, P.J., Bowman, V., Davies, B., Smellie,*
551 *J.L. & Tranter, M (eds). Antarctic Palaeoenvironments and Earth-surface process.*
552 *Geological Society London, Special Publications*, **381**, 7-35.

- 553 Elliot, D. H. & Fleming, T. H. 2000. Weddell Triple Junction: The principal focus of Ferrar and
554 Karoo magmatism during the initial break-up of Gondwana. *Geology*, **28**, 539-542.
- 555 Elliot, D. H. & Fleming, T. H. 2004. Occurrence and Dispersal of Magmas in the Jurassic Ferrar
556 Large Igneous Province, Antarctica. *Gondwana Research*, B, 223-237.
- 557 Elliot, D.H., Fleming, T.H., Haban, M.A. & Siders, M.A. 1995. Petrology and mineralogy of the
558 Kirkpatrick Basalt and Ferrar Dolerite, Mesa Region, Northern Victoria Land, Antarctica. *In*:
559 Elliot, D.H. & Blaisdell, L.L. (eds) *Contribution to Antarctic Research IV*. Antarctic
560 Research Series, 67. American Geophysical Union, Washington DC, 103-141.
- 561 Elliot, D. H., Fleming, T. H., Kyle, P. R. & Foland, K. A. 1999. Long-distance transport of
562 magmas in the Jurassic Ferrar large igneous province, Antarctica. *Earth and Planetary
563 Science Letters*, **167**, 89–104.
- 564 Fleming, T.H., Foland, K.A. & Elliot, D.H. 1995. Isotopic and chemical constraints on the
565 crustal evolution and source signature of Ferrar magmas, north Victoria Land, Antarctica.
566 *Contributions to Mineralogy and Petrology*, **121**, 217-236.
- 567 Galerne, C.Y., Nuemann, E-R. & Planke, S. 2008. Emplacement mechanisms of sill complexes:
568 Information from the geochemical architecture of the Golden Valley Sill Complex, South
569 Africa. *Journal of Volcanology and Geothermal Research*, **177**, 425-440.
- 570 Gibson, S.A., Thompson, R.N., Day, J.A., Humphris, S.E. & Dickin A.P. 2005. Melt-generation
571 associated with the Tristan mantle plume: constraints on the origin of EM-1. *Earth and
572 Planetary Science Letters*, **237**, 744-767.
- 573 Greenway, M. E., 1972. The geology of the Falkland Islands. *British Antarctic Survey Scientific
574 Reports*, **76**, 42 pp.
- 575 Harris, C., Marsh, J.S., Duncan, A.R. & Erlank, A.J. 1990. The Petrogenesis of the Kirwan
576 Basalts of Dronning Maud Land, Antarctica. *Journal of Petrology*, **31**, 341-369.
- 577 Heinonen, J.S. & Luttinen, A.V. 2008. Jurassic dikes of Vestfjella, western Dronning Maud
578 Land, Antarctica: Geochemical tracing of ferropicrite sources. *Lithos*, **105**, 347-364.
- 579 Heinonen, J.S., Carlson, R.W. & Luttinen, A.V. 2010. Isotopic (Sr, Nd, Pb, and Os) composition
580 of highly magnesian dikes of Vestfjella, western Dronning Maud Land, Antarctica: A key to
581 the origins of the Jurassic Karoo large igneous province? *Chemical Geology*, **277**, 227-244.
- 582 Heinonen, J.S., Luttinen, A.V., Riley, T.R. & Nichallik, R.M. 2013. Mixed pyroxenite-
583 peridotite sources for mafic and ultramafic dikes from the Antarctic segment of the Karoo
584 continental flood basalt province. *Lithos*, **177**, 266-380.

- 585 Heinonen, J.S., Carlson, R.W., Riley, T.R., Luttinen, A.V. & Horan, M.F. 2014. Subduction-
586 modified oceanic crust mixed with a depleted mantle reservoir in the sources of the Karoo
587 continental flood basalt province. *Earth and Planetary Science Letters*, **394**, 229-241.
- 588 Hergt J. M., Chappell B. W., Mcculloch M. T., McDougall I. & Chivas A. R. 1989. The
589 geochemistry of Jurassic dolerites from Portal Peak, Antarctica. *Contributions to Mineralogy
590 and Petrology*, **102**, 298-305.
- 591 Herzberg, C. & Asimow, P.D. 2008. Petrology of some oceanic island basalts: PRIMELT2.XLS
592 software for primary magma calculation. *Geochemistry, Geophysics, Geosystems*, **9**.
- 593 Herzberg, C. & Gazel, E. 2009. Petrological evidence for secular cooling in mantle plumes.
594 *Nature*, **458**, 619-623.
- 595 Hole, M.J. 2015. The generation of continental flood basalts by decompression melting of
596 internally heated mantle. *Geology*, **43**.311-314.
- 597 Hole M.J. & Morrison, M.A. 1992. The differentiated boss Cnoc Rhaonastil, Islay; a natural
598 experiment in the low pressure differentiation of an alkali olivine-basalt magma. *Scottish
599 Journal of Geology*, **28**, 55-69.
- 600 Hole, M.J., Millett, J.M., Rogers, N.W. & Jolley, D.W. 2015. Rifting and mafic magmatism in
601 the Hebridean basins. *Journal of the Geological Society, London*, **172**, 218-236.
- 602 Jourdan F., Bertrand H., Schärer U., Blichert-Toft J., Feraud G. & Kampunzu A.B. 2007b.
603 Major and trace element and Sr, Nd, Hf, and Pb isotope compositions of the Karoo large
604 igneous province, Botswana-Zimbabwe: lithosphere vs mantle plume contribution. *Journal
605 of Petrology*, **48**, 1043-1077
- 606 Keiding, J.K., Trumbull, R.B., Veksler, I.V. & Jerram, D.A. 2011. On the significance of ultra-
607 magnesian olivines in basaltic rocks. *Geology*, **39**, 1095-1098.
- 608 Lambart, S., Lapporte, D. & Schiano, P. 2013. Markers of the pyroxenite contribution in the
609 major-element compositions of oceanic basalts: Review of the experimental constraints.
610 *Lithos*, **160-161**, 14-36.
- 611 Luttinen, A.V. & Furnes, H., 2000. Flood basalts of the Vestfjella: Jurassic magmatism across
612 an Arcehan-Proterozoic lithospheric boundary in Dronning Maud Land, Antarctica. *Journal
613 of Petrology*, **41**, 1271-1305.
- 614 Luttinen, A.V., Ramo, O.T. & Huhma, H. 1998. Neodymium and strontium isotope and trace
615 element composition of a Mesozoic CFB suite from Dronning Maud Land, Antarctica:
616 implications for lithosphere and asthenosphere contributions to Karroo magmatism.
617 *Geochimica et Cosmochimica Acta*, **15**, 2701-2714.

- 618 Macdonald, D.I.M., Gomez-Perez, I., Franzese, J., Spalleti, L., Lawver, L., Gahagan, L.,
619 Dalziel, I.W.D., Thomas, C.J., Trewin, N.H., Hole, M.J. & Paton, D. 2003. Mesozoic break-
620 up of SW Gondwana: implications for regional hydrocarbon potential of the southern South
621 Atlantic. *Marine & Petroleum Geology*, **20**, 287-308
- 622 Marsh, J.S., Hooper, P.R., Rehacek, J., Duncan, R.A. & Duncan, A.R. 1997. Stratigraphy and
623 age of Karroo basalts of Lesotho and implications for correlations within the Karroo
624 Igneous Province. In: Mahoney, J.J. & Coffin, M.F. (eds) *Large Igneous Provinces*, A G U
625 Geophysical Monographs, 100, 247-272.
- 626 McClintock, M., Marsh, J. & White, J.D.L. 2008. Compositionally diverse magmas erupted
627 close together in space and time within a Karroo flood basalt crater complex. *Bulletin of*
628 *Volcanology*, **70**, 923-946.
- 629 Mitchell, C., Ellam, R.M. & Cox, K.G. 1999. Mesozoic dolerite dykes of the Falkland Islands:
630 petrology, petrogenesis and implications for geochemical provinciality in Gondwanaland
631 low-Ti basaltic rocks. *Journal of the Geological Society, London*, **156**, 901-916.
- 632 Molzahn, M., Reisberg, L. & Wörner, G. 1996. Os, Sr, Nd, Pb, O isotope and trace element
633 data from the Ferrar flood basalts, Antarctica: evidence for an enriched subcontinental
634 lithospheric source. *Earth and Planetary Science Letters*, **144**, 529-546.
- 635 Muirhead, J.D., Airoidi, G., White, J.L. and Rowland, J.V. 2014. Cracking the lid: Sill-fed
636 dikes are the likely feeders of flood basalt eruptions. *Earth and Planetary Science Letters*,
637 **406**, 187-197.
- 638 Mussett, A.E. & Taylor, G.K. 1994. ^{40}Ar - ^{39}Ar ages for dykes from the Falkland Islands with
639 implications for the break-up of southern Gondwanaland. *Journal of the Geological Society*,
640 *London*, **151**, 79-81.
- 641 Nuemann, E-R., Svensen, H., Galerne, G.Y. & Planke, S. 2011. Multistage Evolution of
642 Dolerites in the Karroo Large Igneous Province, Central South Africa. *Journal of Petrology*,
643 **52**, 959-984.
- 644 Putirka, K.D., Perfit, M., Ryerson, F.J. & Jackson, M.G. 2007. Ambient and excess mantle
645 temperatures, olivine thermometry, and active vs. passive upwelling. *Chemical Geology*, **241**,
646 177-206.
- 647 Richards, P.C., Stone, P., Kimbell, G.S., Mcintosh, W.C. & Phillips, E.R. 2013. Mesozoic
648 magmatism in the Falkland Islands (South Atlantic) and their offshore sedimentary basins.
649 *Journal of Petroleum Geology*, **36**, 61-74.

- 650 Riley, T.R., Curtis, M.L., Leat, P.T., Watkeys, M.K., Duncan, R.A., Millar, I.L. & Owens, W.H.
651 2006. Overlap of Karoo and Ferrar Magma Types in KwaZulu-Natal, South Africa.
652 *Journal of Petrology*, **47**, 541-566.
- 653 Sato, M., Shuto, K., Nohara-Imanaka, R., Takazawa, E., Osanai, Y. & Nakano, N. 2014.
654 Repeated magmatism at 34 Ma and 23-20 Ma producing highmagnesian adakitic andesites
655 and transitional basalts on southern Okushiri Island, NE Japan arc. *Lithos*, **205**, 60-83.
- 656 Sushchevskaya, N.M., Korago, E.A., Belyatsky, B.V. & Sirotkin, A.N. 2009. Evolution of the
657 Karoo-Maud mantle plume in Antarctica and its influence on the magmatism of the early
658 stages of Indian ocean opening. *Geochemistry International*, **47**, 1-17.
- 659 Stone, P., Kimbell, G.S. & Richards, P.C. 2009. Rotation of the Falklands microplate reassessed
660 after recognition of discrete Jurassic and Cretaceous dyke swarms. *Petroleum Geoscience*,
661 **15**, 279-287.
- 662 Stone, P., Richards, P.C., Kimbell, G.S., Esser, R.P., & Reeves, D. 2008 Cretaceous dykes
663 discovered in the Falkland Islands: implications for regional tectonics in the South Atlantic.
664 *Journal of the Geological Society, London*, **165**, 1-4
- 665 Storey, B.C., Alabaster, T., Hole, M.J., Pankhurst, R.J. & Wever, H. 1992. Role of subduction-
666 plate boundary forces during the initial stages of Gondwana break-up: Evidence from the
667 proto-Pacific margin of Antarctica. In: Storey, B. C., Alabaster, T. & Pankhurst, R. J. (eds)
668 *Magmatism and the causes of Continental Break-Up* Geological Society, London, Special
669 Publications, **64**, 149-163.
- 670 Sweeney R. J., Duncan A. R., Erlank A. J. 1994. Geochemistry and Petrogenesis of Central
671 Lebombo basalts of the Karoo igneous province. *Journal of Petrology*, **35** 95-125.
- 672 Sun, S-S. & McDonough, W. F. 1989. Chemical and isotopic systematics of oceanic basalts:
673 implications for mantle composition and processes. In: Saunders, A.D. & Norry, M.J.,
674 (eds). *Magmatism in the ocean basins*. Geological Society, London, Special Publications,
675 **42**, 313-345.
- 676 Sushchevskaya, N. M., Belyatskii, B. V., Leichenov, G. L. & Laiba A. A. 2009. Evolution of the
677 Karoo-Maud plume in Antarctica and its influence on the magmatism of the early stages of
678 Indian Ocean opening. *Geochemistry International*, **47**, 1-17
- 679 Svensen, H., Corfu, F., Polteau, S., Hammer, O & Planke, S. 2012. Rapid magma emplacement
680 in the Karoo Large Igneous Province. *Earth and Planetary Science Letters*, **325-326**, 1-9.
- 681 Thistlewood, L., Leat, P. T., Millar, I.L., Storey, B.C. & Vaughan, A. P. M. 1997. Basement
682 Geology and Palaeozoic-Mesozoic mafic dykes from the Cape Meredith Complex, Falkland

- 683 Islands: a record of repeated intracontinental extension. *Geological Magazine*, **134**, 355-
684 367.
- 685 Thompson, R.N., Gibson, S.A., Dickin, A.P. & Smith, P.M. 2001. Early Cretaceous basalt and
686 picrate dykes of the Southern Etendeka region, NW Namibia: windows into the role of the
687 Tristan plume in Parana-Etendeka magmatism. *Journal of Petrology*, **42**, 2049-2081.
- 688 Trewin, N.H., Macdonald, D.I.M., & Thomas, C.G.C. 2002. Stratigraphy and sedimentology of
689 the Permian of the Falkland Islands: lithostratigraphic and palaeoenvironmental links with
690 South Africa. *Journal of the Geological Society, London*, **159**, 5–19.
- 691 Villiger, S., Ulmer, P. & Muntener, O. 2007. Equilibrium and fractional crystallization
692 experiments at 0.7 GPa; the effect of pressure on phase relations and liquid compositions of
693 tholeiitic magmas. *Journal of Petrology*, **48**, 159-184.
- 694 Wilhelm, S. & Wörner, G. 1996. Crystal size distribution in Jurassic Ferrar flows and sills
695 (Victoria Land, Antarctica): evidence for processes of cooling, nucleation and
696 crystallization. *Contributions to Mineralogy and Petrology*, **125**, 1-15.
- 697 Williamson, I.T. & Bell, B.R. 2012. The Staffa Lava Formation: graben-related volcanism,
698 associated sedimentation and landscape character during the early development of the
699 Palaeogene Mull Lava Field, NW Scotland. *Scottish Journal of Geology*, **48**, 1-46.
- 700

701 **Figure Captions**

702 Figure 1. a) Reconstruction of Southern Gondwana showing the position of the Falkland Islands
703 relative to south-eastern Africa prior to continental break-up. The three arrows represent the
704 main dyke trends on the Falkland Islands rotated back to their pre-180 Ma orientation. After
705 Trewin *et al.* (2002). b) Southern Gondwana, in the Middle Jurassic, showing the distribution of
706 Jurassic break-up related magmas in southern Africa and Antarctica. MEB, Maurice Ewing
707 Bank; EWM, Ellsworth-Whitmore Mountains; AP, Antarctic Peninsula; SA, South Africa;
708 SAM, South America; ANT, Antarctica. Position of the Weddell, Limpopo and Lower Zambesi
709 triple junctions are from Elliot & Fleming (2000). Ar-Ar ages, this study and Stone *et al.* (2009).
710 After Macdonald *et al.* (2003). Key to shading for Fig. 1b is the same as that for Fig. 1a.

711 Figure 2. Map of the Falkland Islands showing the distribution of magnetic anomalies and main
712 trends of dyke swarms. Solid or pecked lines do not necessarily represent continuous exposure
713 of dykes. Inset; azimuths of Dykes in the South Harbour area of West Falkland. The rectangle at
714 South Harbour is the area covered by the map in the supplementary material, which gives the
715 sample locations and geochemical type to which the dykes belong in that area. After Stone *et al.*
716 *et al.* (2009) and Richards *et al.* (2013). Ar-Ar ages (this study, Stone *et al.* 2008; 2009) and
717 sample locations which are mentioned in the text, are indicated, along with the geochemical
718 group to which the intrusions belong, given by the following abbreviations; PST, Port Sussex
719 Type; MAT, Mount Alice Type, E-W, East-West Type of Mitchell *et al.* (1999); DIT, Dyke
720 Island Type. Identifying characteristics of each type of intrusion are discussed in detail in the
721 text.

722 Figure 3. Ar-Ar step-heating spectrum for plagioclase in sample WI-5. Full data are given in the
723 supplementary materials.

724 Figure 4. Major (wt%) and trace element (in ppm) variations *versus* MgOwt% in Falkland
725 Islands dykes. Filled dots, Port Sussex Creek type (PST) NE-SW two-pyroxene dolerites; open
726 triangles, E-W olivine dolerite dykes; open squares, Lively Island dyke; filled squares, Mount
727 Alice-type (MAT) dykes; open dots, low TiO₂ DIT intrusions; filled diamonds, high TiO₂ DIT
728 intrusions; open diamonds, evolved sheets from the South Harbour-Dyke Island transect (Dyke
729 Island Type; DIT); crosses, Pony's Pass N-S Cretaceous dyke (Stone *et al.* 2008). Data from this
730 study, Mitchell *et al.* (1999) and Thistlewood *et al.* (1997).

731 Figure 5. Pyroxene end-member compositions represented in the quadrilateral system Enstatite -
732 Ferrosilite – Wollastonite for Falkland Islands intrusions (this study and Mitchell *et al.* 1999)
733 and dolerites from the Transantarctic Mountains (Elliot 1995; Demarchi *et al.* 2001). MFCT,

734 Mount Fazio Chemical Type; SPCT, Scarab Peak Chemical Type; NVL, Northern Victoria
735 Land.

736 Figure 6. Chondrite-normalized REE profiles for representative samples of a) DIT intrusions
737 and b) PST, MAT and E-W intrusions.

738 Figure 7. a) to d) Multi-element ORB-normalized (Sun & McDonough 1989) variation diagrams
739 for Falkland Islands dykes. Comparable basalts from other regions of the low TiO₂ Gondwana
740 LIP are shown by grey lines. Sample SA.6.1 (South Africa), Riley *et al.* (2006); VF111-85, CT3
741 basalt, Dronning Maud Land (Luttinen & Furnes 2000); 47206-3, low TiO₂ tholeiite from
742 Schirmacher Oasis, Dronning Maud Land (Sushchevskaya *et al.* 2009); Average MFCT from
743 Elliot *et al.* (1995).

744 Figure 8. a) ϵNd_{182} versus $^{87}\text{Sr}/^{86}\text{Sr}_{182}$; b) $^{207}\text{Pb}/^{204}\text{Pb}$ versus $^{206}\text{Pb}/^{204}\text{Pb}$ for Falkland Islands
745 dykes. c) ϵNd_{182} versus $^{207}\text{Pb}/^{204}\text{Pb}$ for Falkland Islands intrusions. Symbols as for Fig. 4. Data
746 sources this study, Mitchell *et al.* (1999) and Thistlewood *et al.* (1997).

747 Figure. 9 a) ϵNd_{182} versus MgO; b) ϵNd_{182} versus Th/Ta and c) $^{87}\text{Sr}/^{86}\text{Sr}_{182}$ versus 1/Sr for
748 Falkland Islands intrusions. Symbols as for Fig. 4 except grey dots are for the lowest reported
749 Th/Ta for Ferrar dolerites (Fleming *et al.* 1995). Parameters for the AFC mixing line are given
750 in Table 4 with % AFC given on the mixing line.

751 Figure 10. Ti/Zr versus SiO₂ for Falkland Islands dykes. Symbols as for Fig. 4.

752 Figure 11. TiO₂ versus MgO, for Falkland Islands dykes the Ferrar LIP and igneous rocks
753 considered to be transitional between the compositions of Ferrar and Karoo magmas. Data
754 sources; Hergt *et al.* (1989), Brewer *et al.* (1992), Elliot *et al.* (1995), Fleming *et al.* (1995),
755 Molzahn *et al.* (1996), Wilhelm & Worner (1996), Antonini *et al.* (1999), Elliot *et al.* (1999),
756 Elliot & Fleming (2004), Riley *et al.* (2006). Falkland Islands samples symbols as for Fig. 4.

757 Fig. 12. ϵNd_{182} versus $^{87}\text{Sr}/^{86}\text{Sr}_{182}$ for Falkland Islands PST intrusions (filled dots) Karoo low
758 TiO₂ volcanic rocks (open circles), Dronning Maud Land CT1 (open triangles), CT2 (filled
759 diamonds) and CT3 (filled triangles) basalts. Details of the parameters used in generating the
760 three AFC mixing lines (CT1, PST-1 and PST-2) are given in Table 4. Each cross represents 1%
761 AFC. Data sources for Karoo Province; Galerne *et al.* (2008); McClintock *et al.* (2008);
762 Neumann *et al.* (2011).

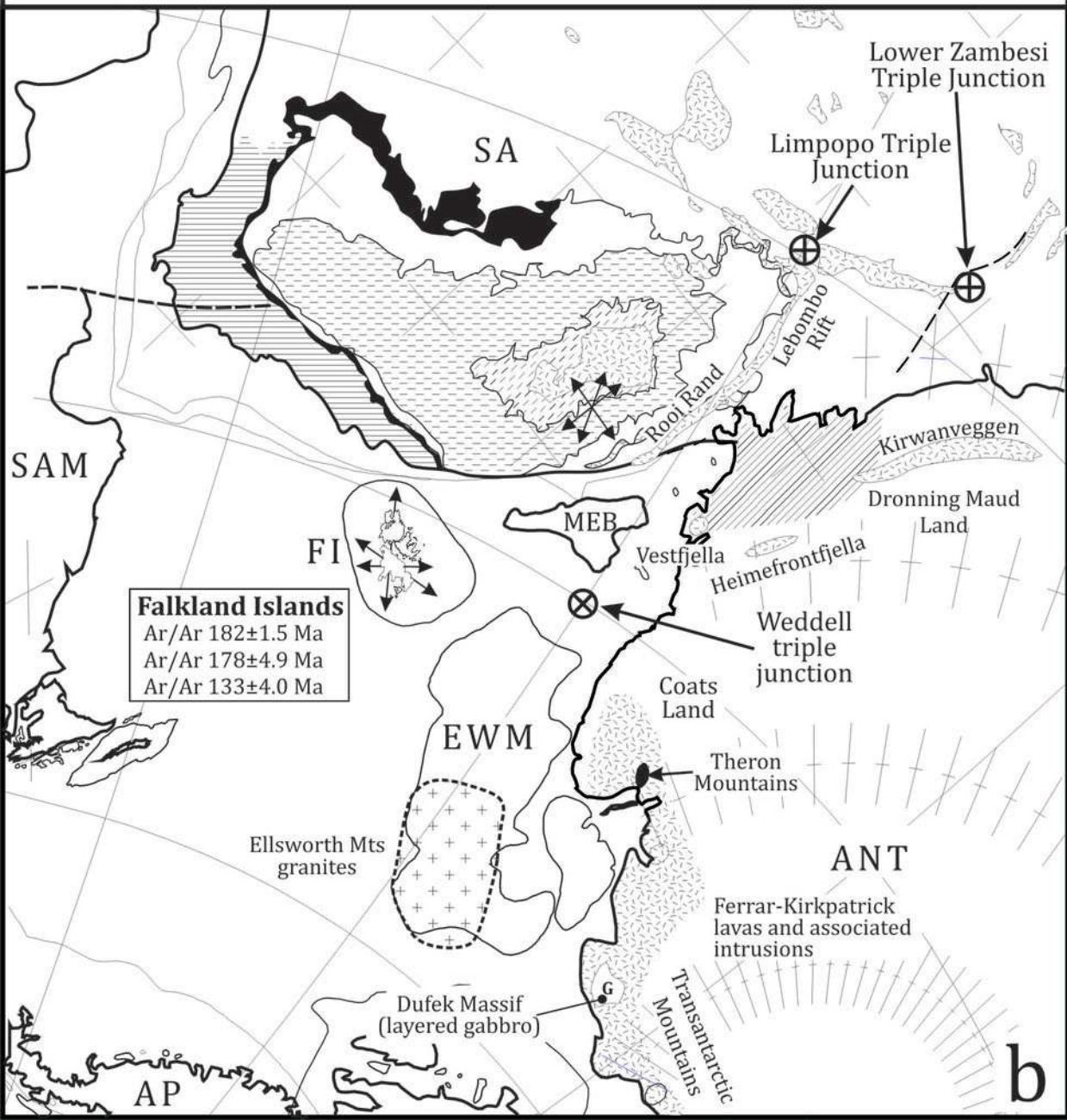
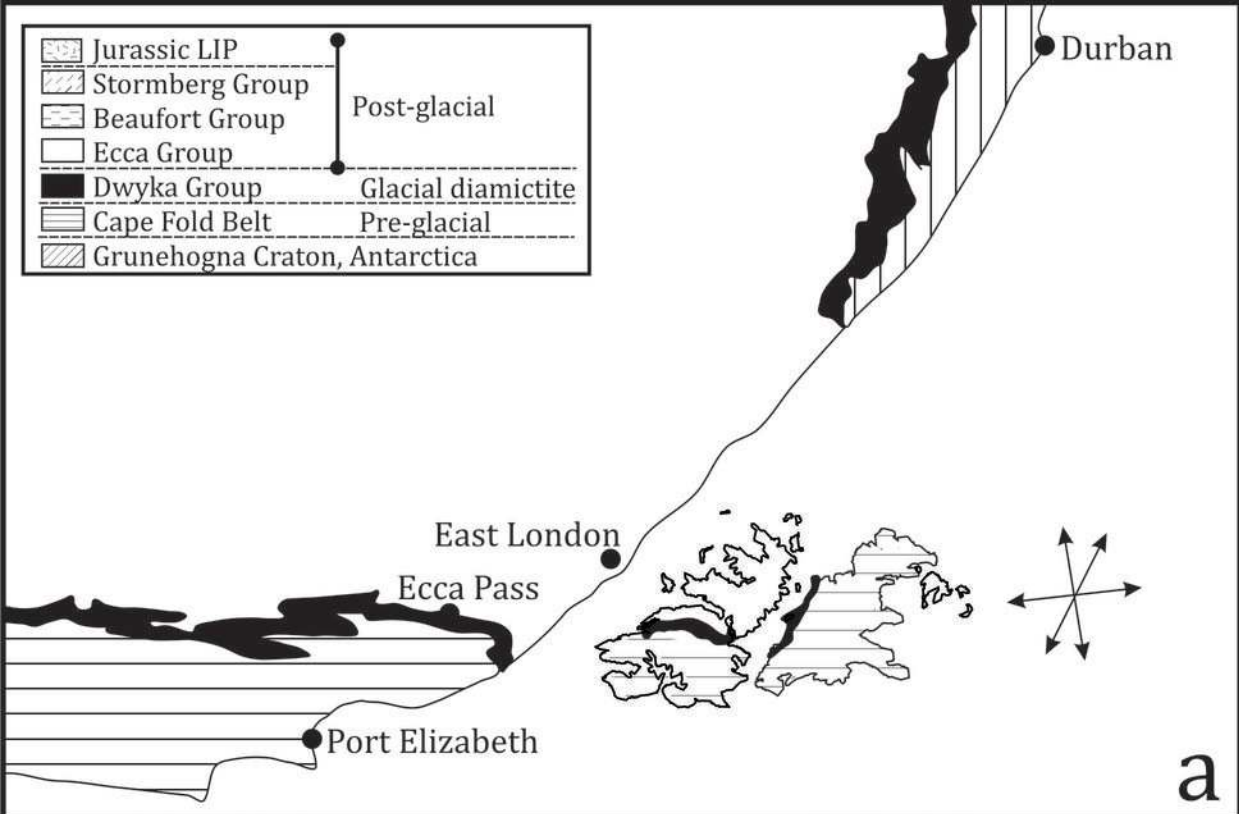
763 Figure 13. a) CaO versus MgO (weight %) for Falkland Islands intrusions (black dots PST; grey
764 dots, DIT; grey squares MAT; triangles, E-W) and Dronning Maud Land high MgO, silica-

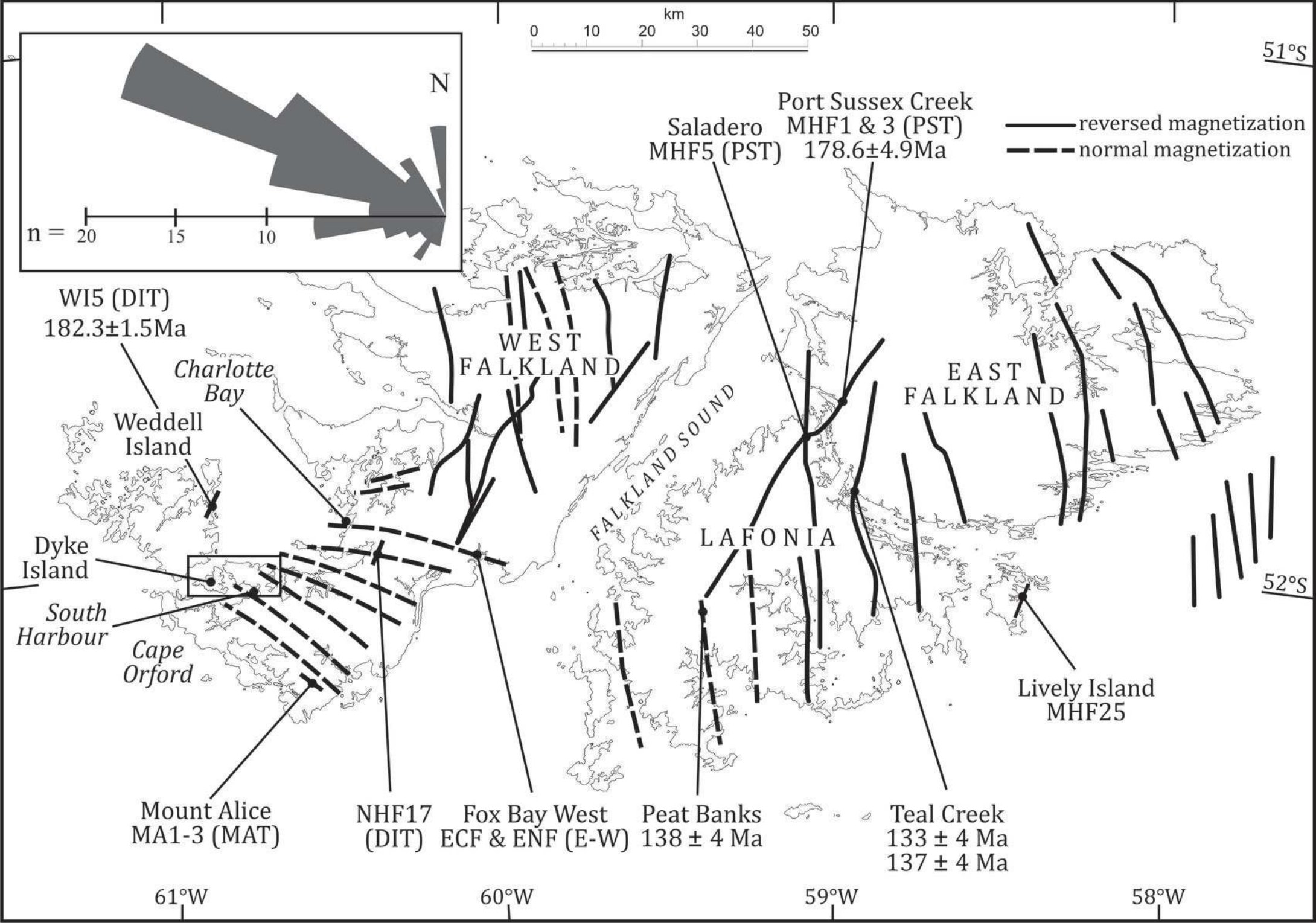
765 oversaturated CT1 basalts (circles). The dividing line between melts derived from peridotite
766 and pyroxenite sources is taken from Herzberg & Asimow (2008). Lines with crosses and
767 arrows represent the effect of accumulation of the phase indicated on the composition of PST
768 basalt NEF9, with each cross representing 5% accumulation. b) Cr (ppm) *versus* SiO₂ for
769 Falkland Islands intrusions (symbols as for Fig. 4) and high-Mg andesites from Mt Shasta
770 (crosses; Baker *et al.* 1994).

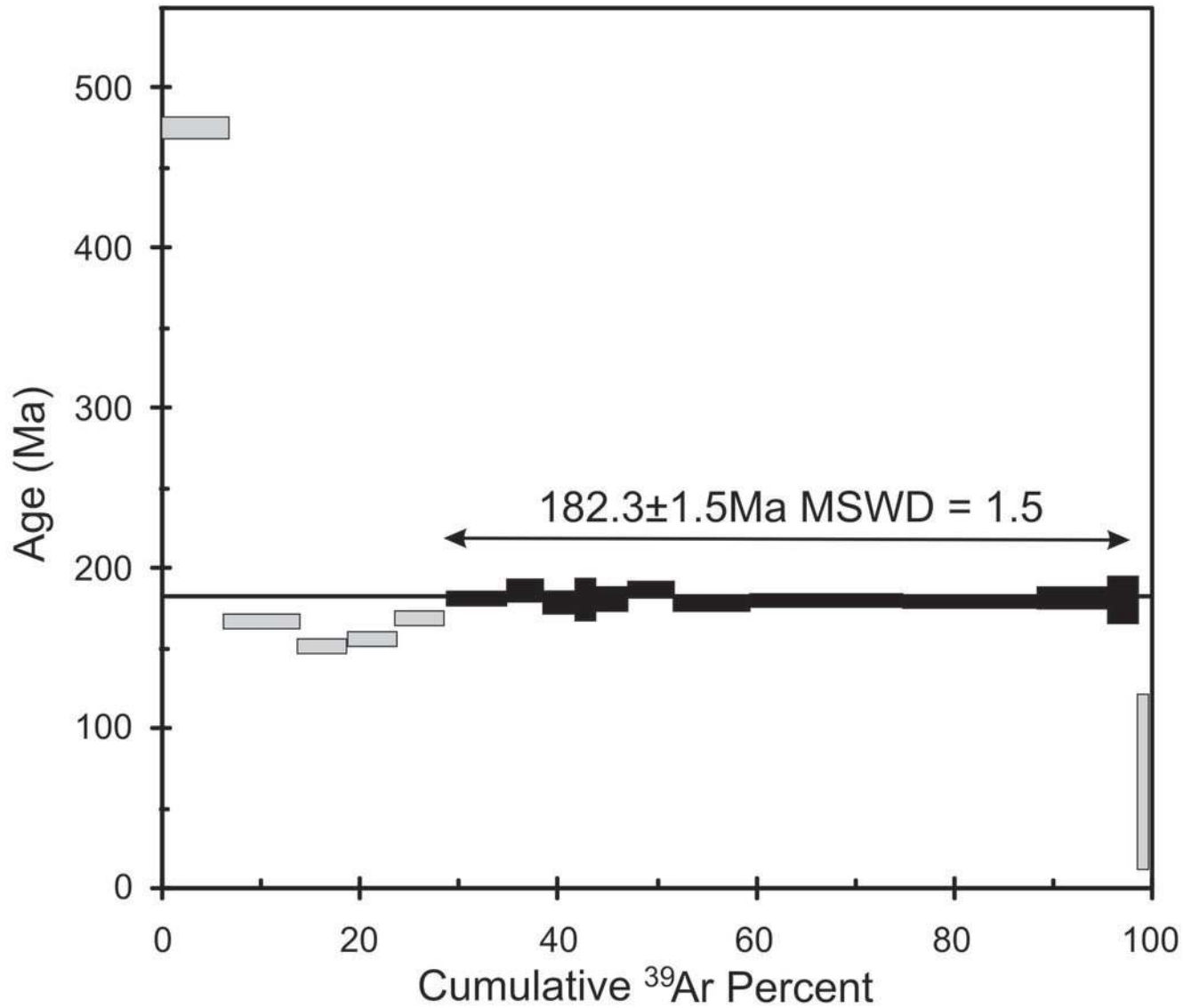
771 Figure 14. Ti/Zr *versus* SiO₂, for a) Karoo LIP volcanic rocks and b) Ferrar LIP volcanic rocks.
772 Note that the KwaZulu-Natal and Theron Mountains low TiO₂ samples are considered to be
773 magma types transitional between Karoo and Ferrar types. Data sources; Transantarctic
774 Mountains and Theron Mountains; Hergt *et al.* (1989), Brewer *et al.* (1992), Elliot *et al.* (1995),
775 Fleming *et al.* (1995), Molzahn *et al.* (1996), Wilhelm & Worner (1996), Antonini *et al.* (1999),
776 Elliot *et al.* (1999), Elliot & Fleming (2004). Karoo (including Dronning Maud Land) Luttinen
777 *et al.* (1998), Luttinen & Furnes (2000), Heinonen & Luttinen (2008), Heinonen *et al.* (2010;
778 2013; 2014) Neumann *et al.* (2011). Kirwanveggan; Harris *et al.* (1990).

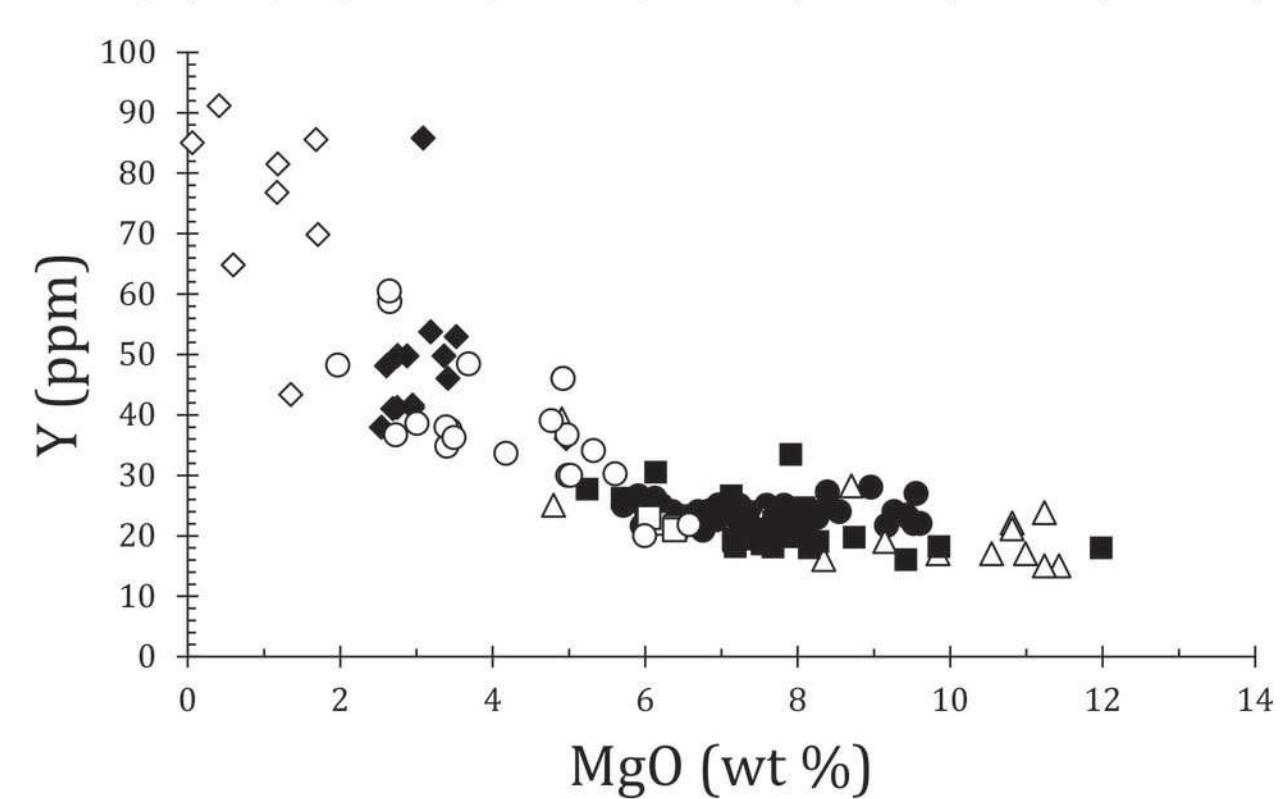
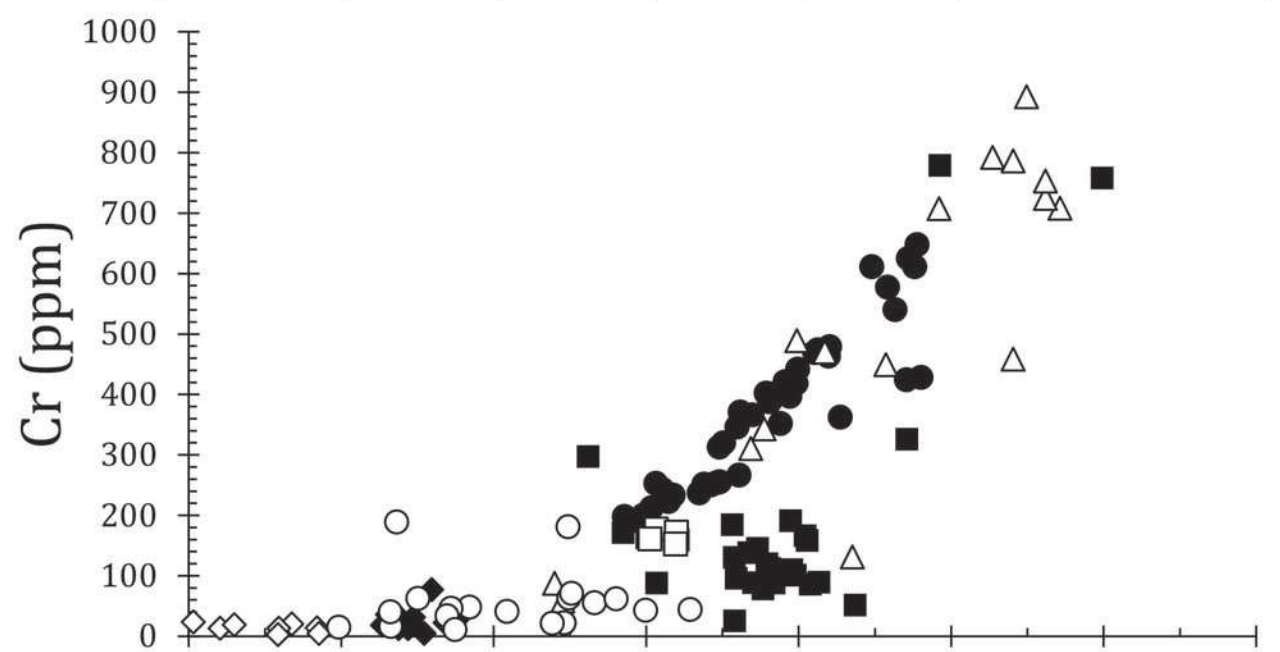
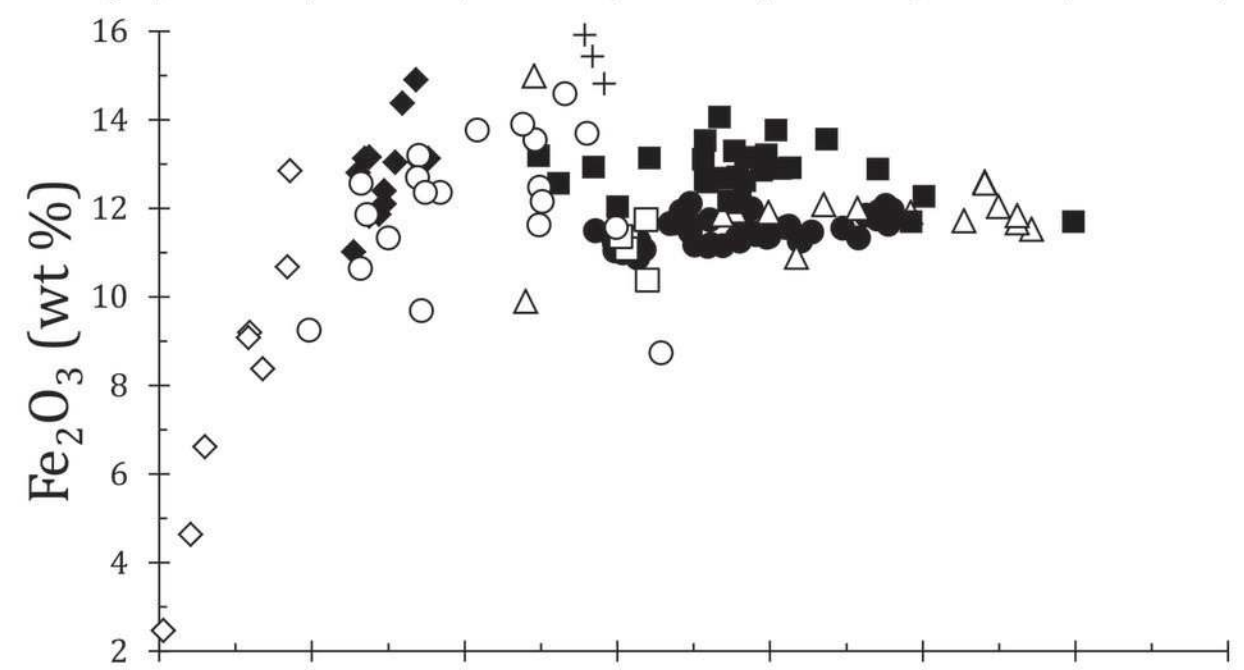
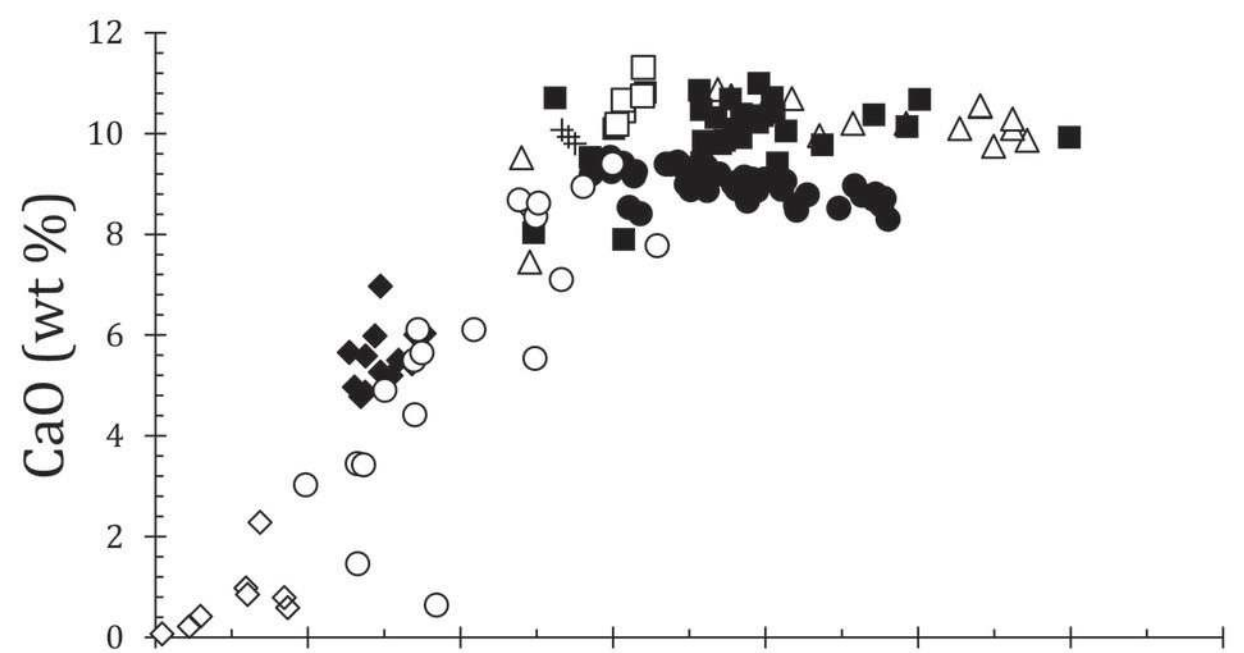
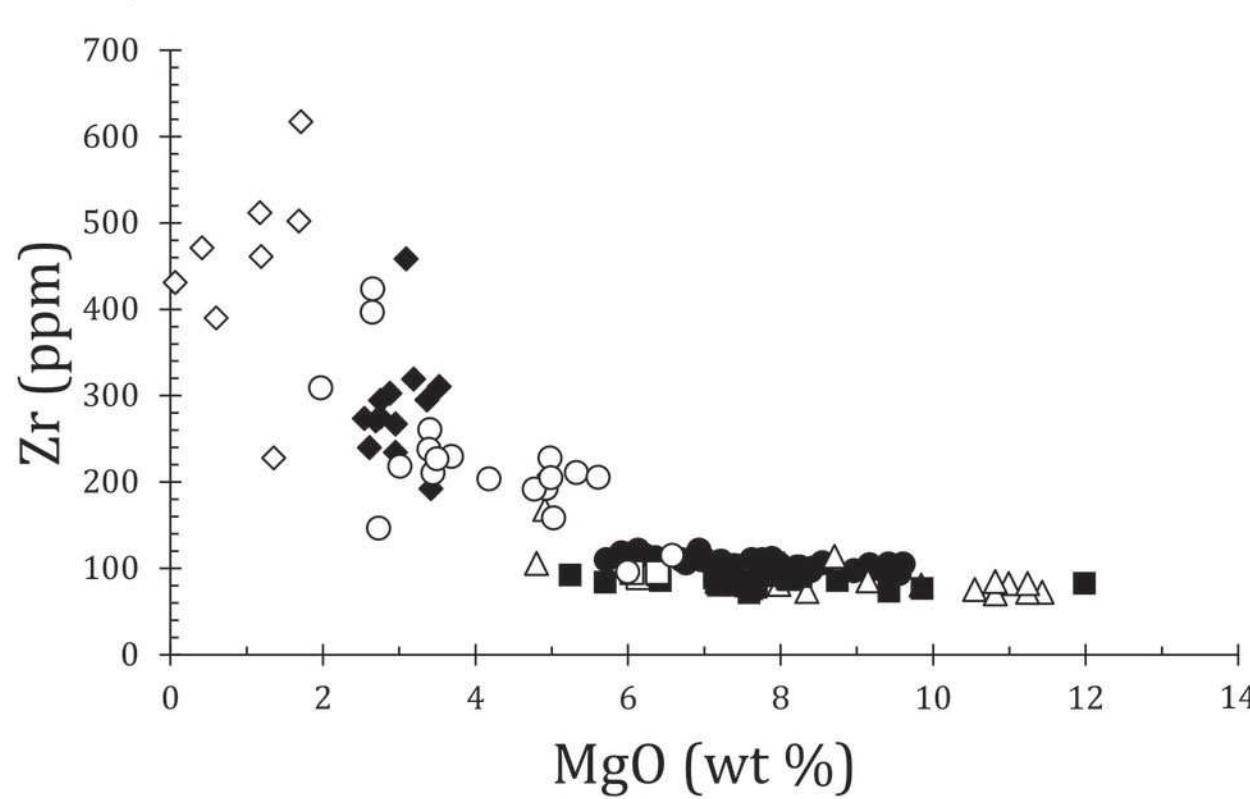
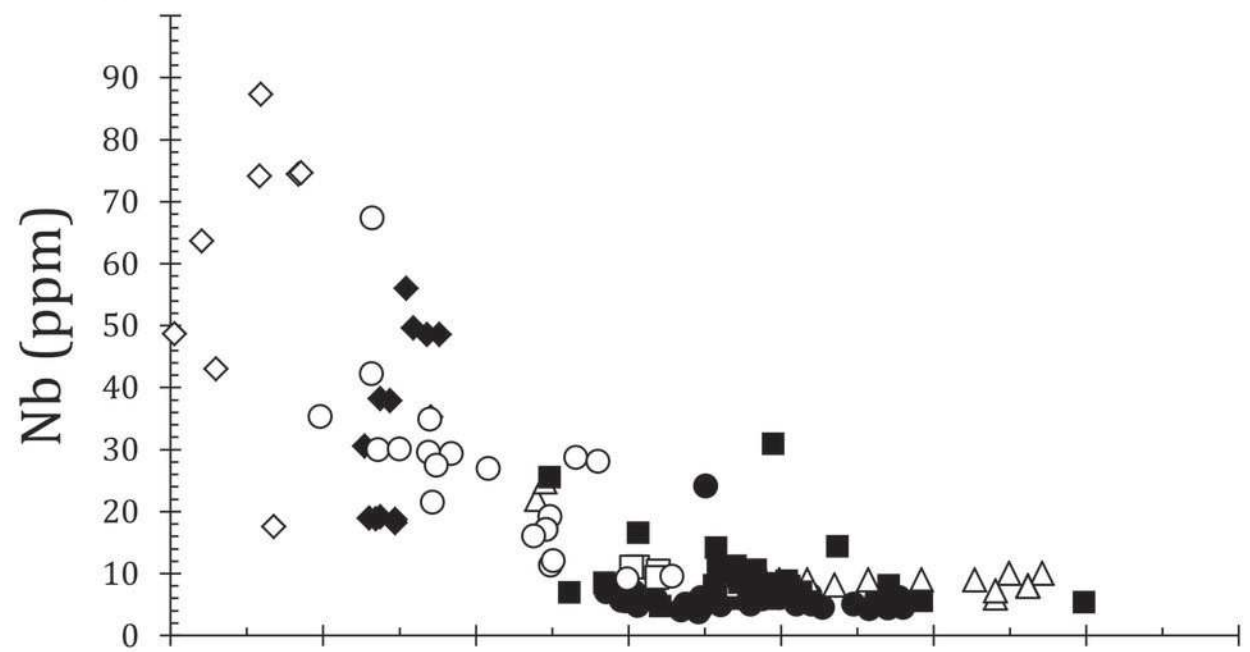
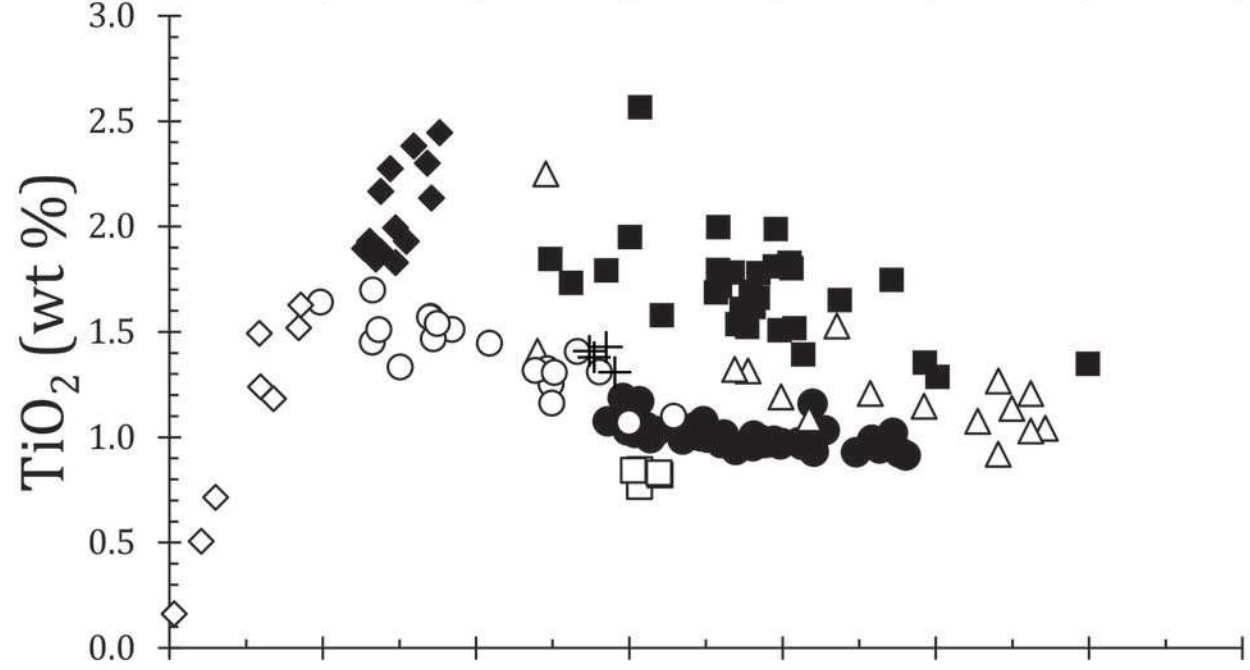
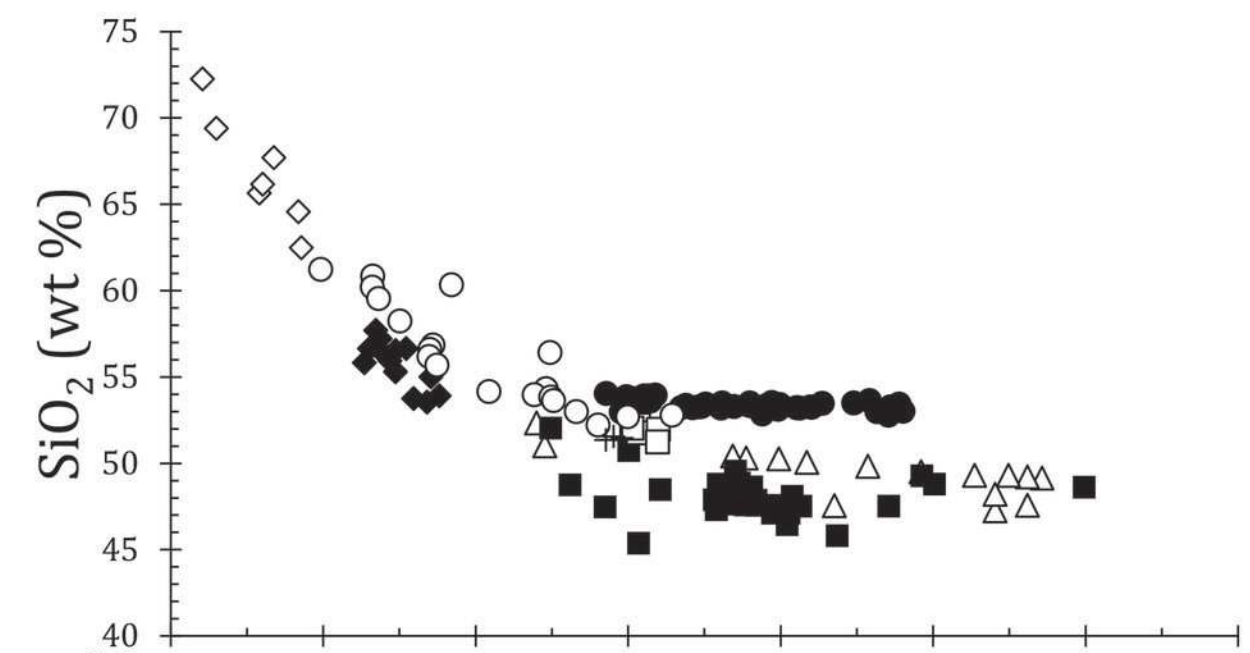
779 Figure 15. a) Olivine equilibration temperatures (°C) *versus* Mg# of liquid in equilibrium with
780 olivine for Ahlmannryggen dykes (filled dots; Heinonen & Luttinen 2008), Vestfjella high TiO₂
781 ferropicrite (filled triangles; Heinonen *et al.* 2013), Etendeka picrite (open squares; Kieding *et*
782 *al.* 2011) and Falklands Islands MAT intrusion (star in circle) and E-W intrusions (open
783 triangles). Olivine equilibration temperatures have been calculated according to the scheme of
784 Putirka *et al.* (2007). Vertical lines connecting points for Ahlmannryggen samples are calculated
785 equilibration temperatures for different olivine phenocrysts in individual whole-rock samples.
786 Figures in italics are T_p from melt inclusions for Etendeka samples plotted in Fig. 15a (Kieding
787 *et al.* 2011). b) Inferred temperature-pressure conditions at which fractional melting terminated
788 for calculated primary magmas from Dronning Maud Land, the Karoo Province of southern
789 Africa, Ferrar dolerites of Antarctica and picrites of the Etendeka Province of western Africa.
790 The diagram was constructed following the methods of Herzberg and Gazel (2009) with data for
791 the Ferrar province and Iceland from Hole (2015). Samples with MgO > 20 weight % are
792 shown schematically following an adiabatic pathway for T_p = 1640°C. The diagonally shaded
793 box on the temperature axis is the range of olivine equilibration temperatures, calculated at 0
794 GPa, for olivine in ferro-picrite dykes from Dronning Maud following the method of Putirka *et*
795 *al.* (2007), and the box labelled 'MAT & E-W' is the same calculations for MAT and E-W
796 intrusions. Adiabatic melting paths are labelled with mantle potential temperature. 2σ error bars
797 are from Hole (2015). c) T_p calculated from melt inclusions in ultra-magnesian olivines from the

798 Etendeka Province *versus* olivine equilibration temperatures for the same samples. Data from
799 Keiding *et al.* (2011).
800







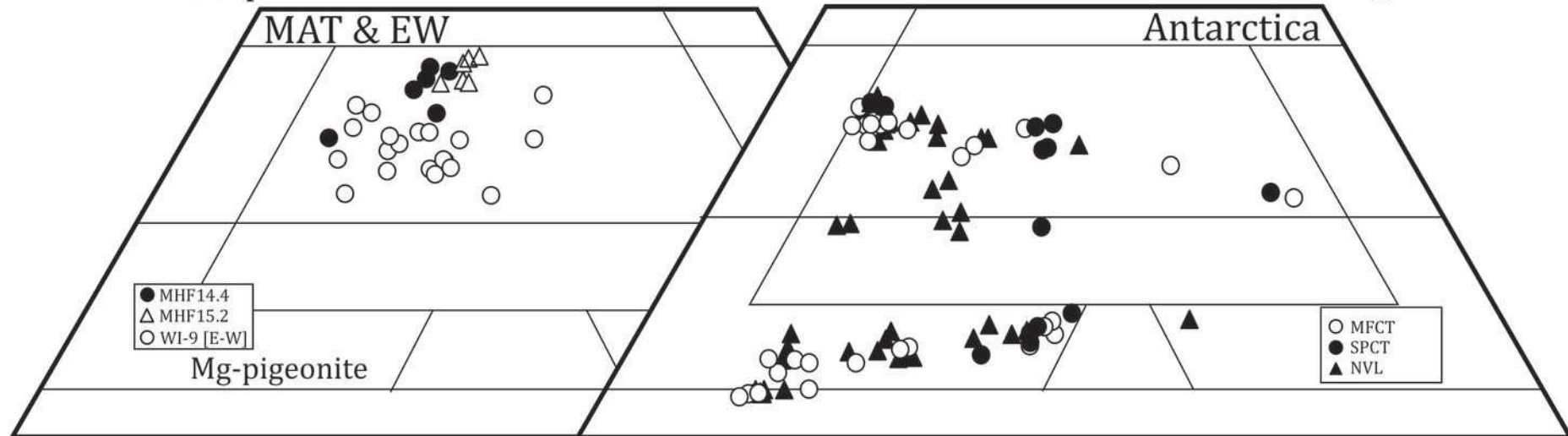


Diopside

Hedenbergite

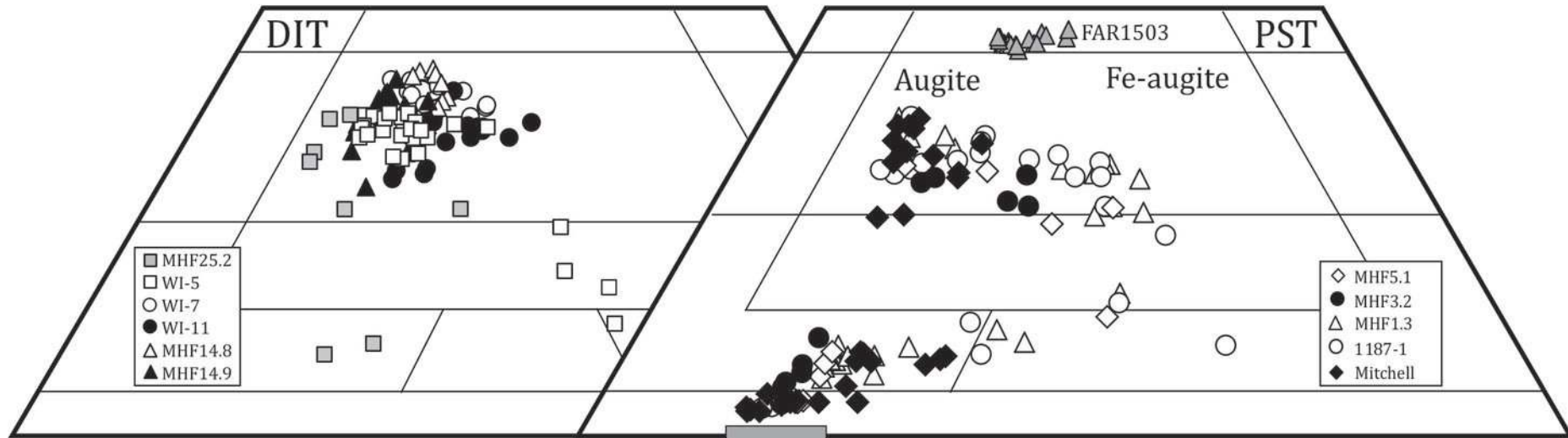
MAT & EW

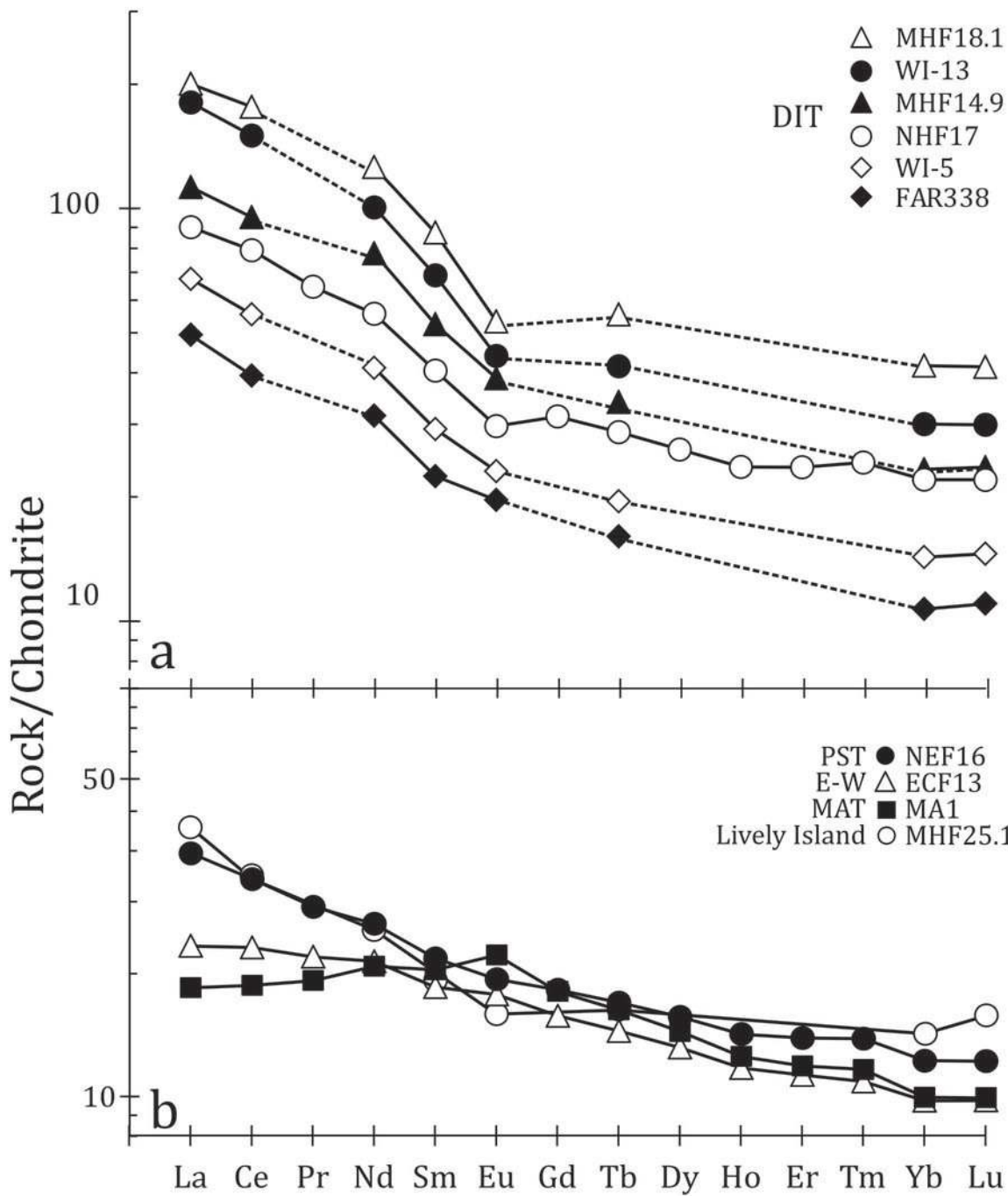
Antarctica

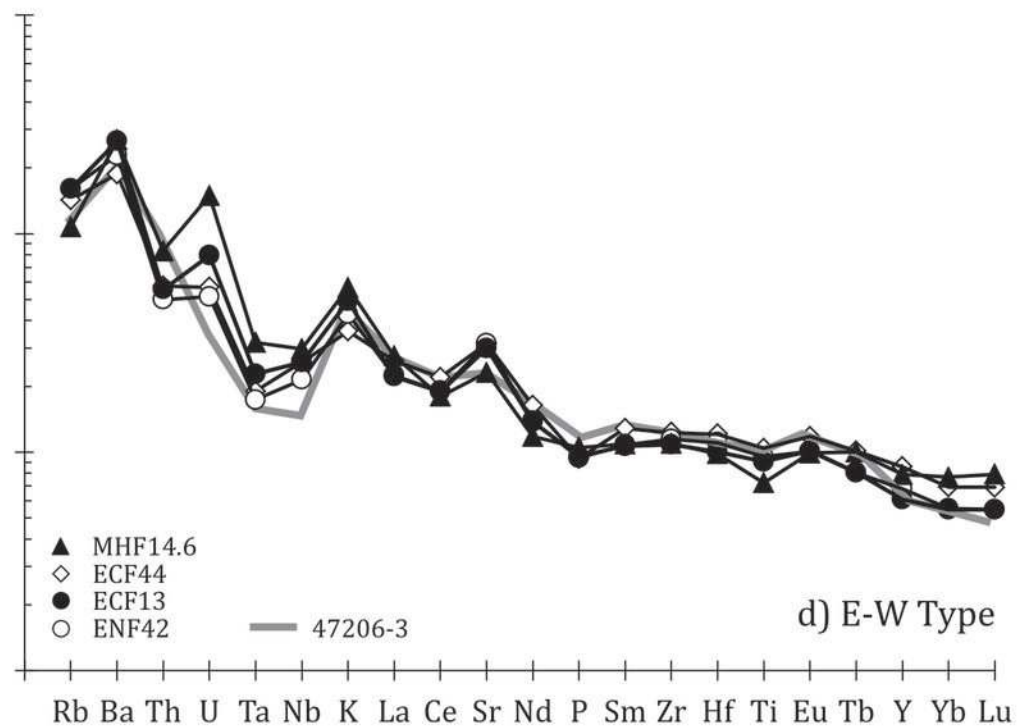
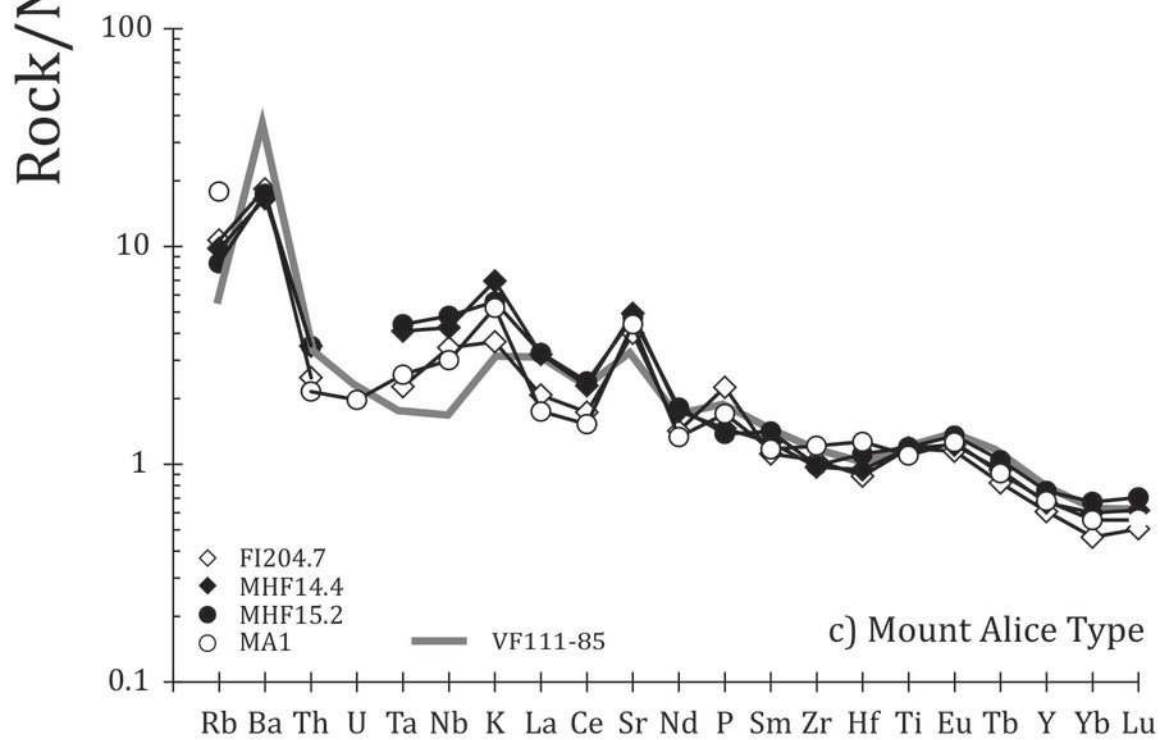
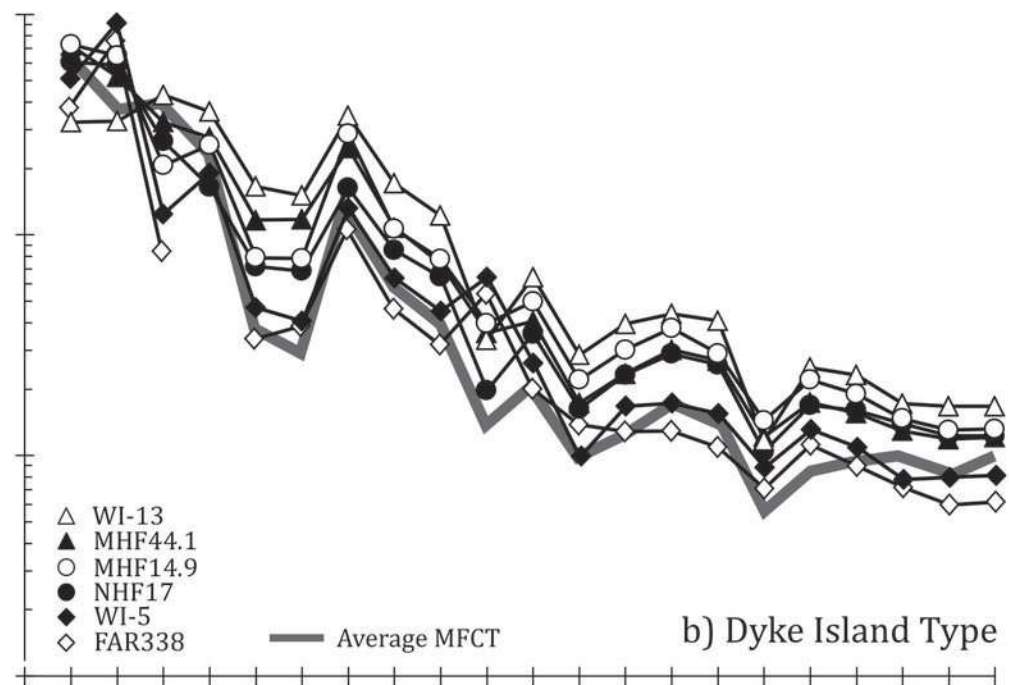
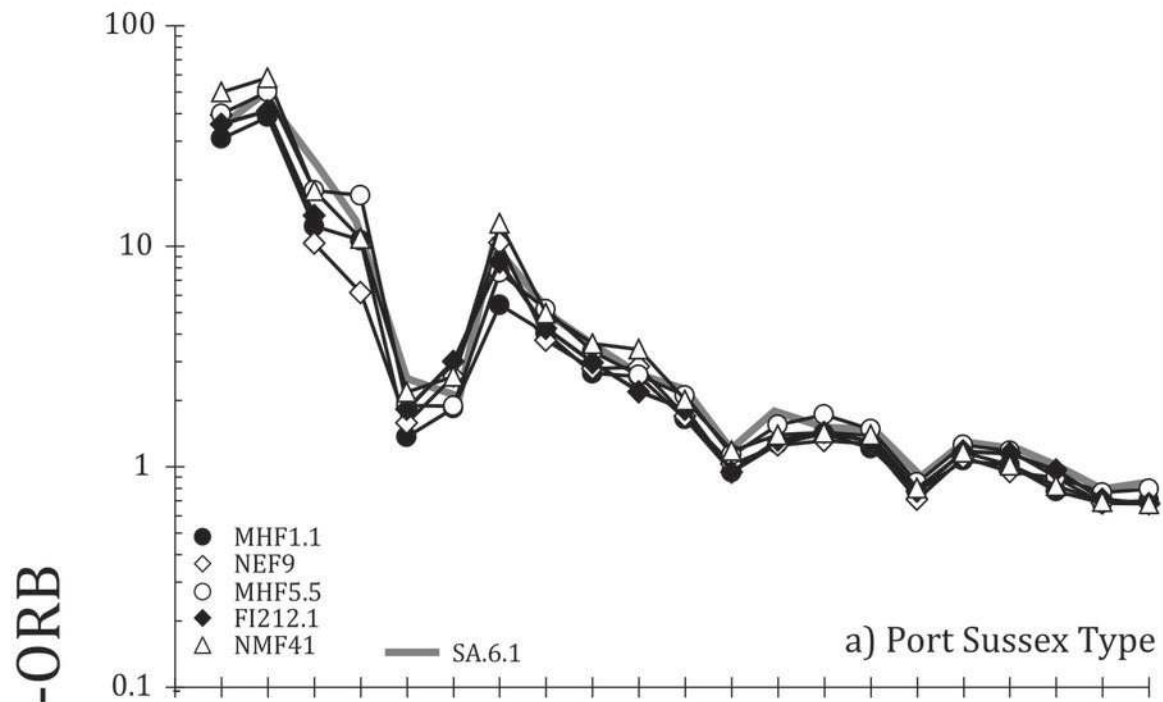


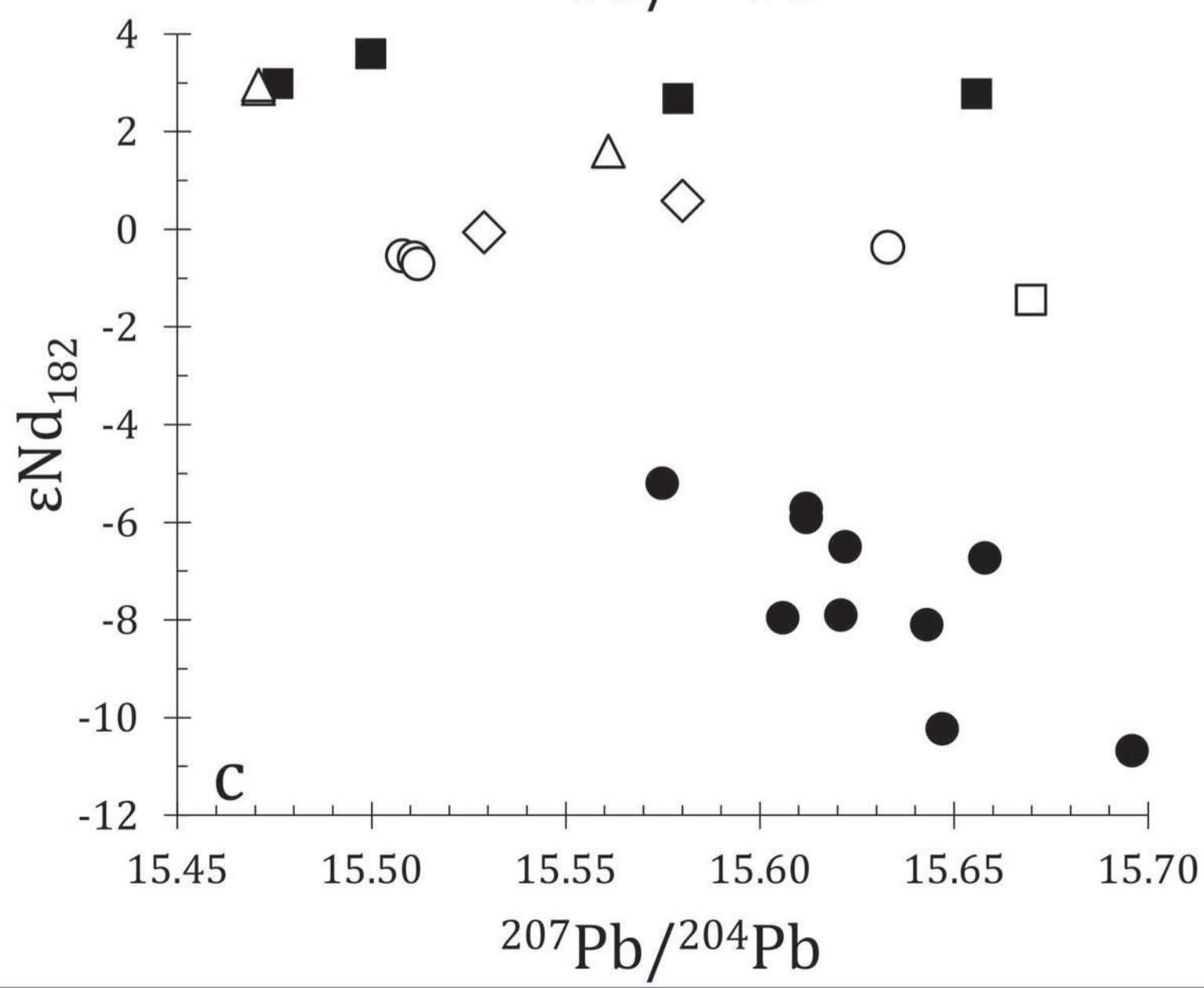
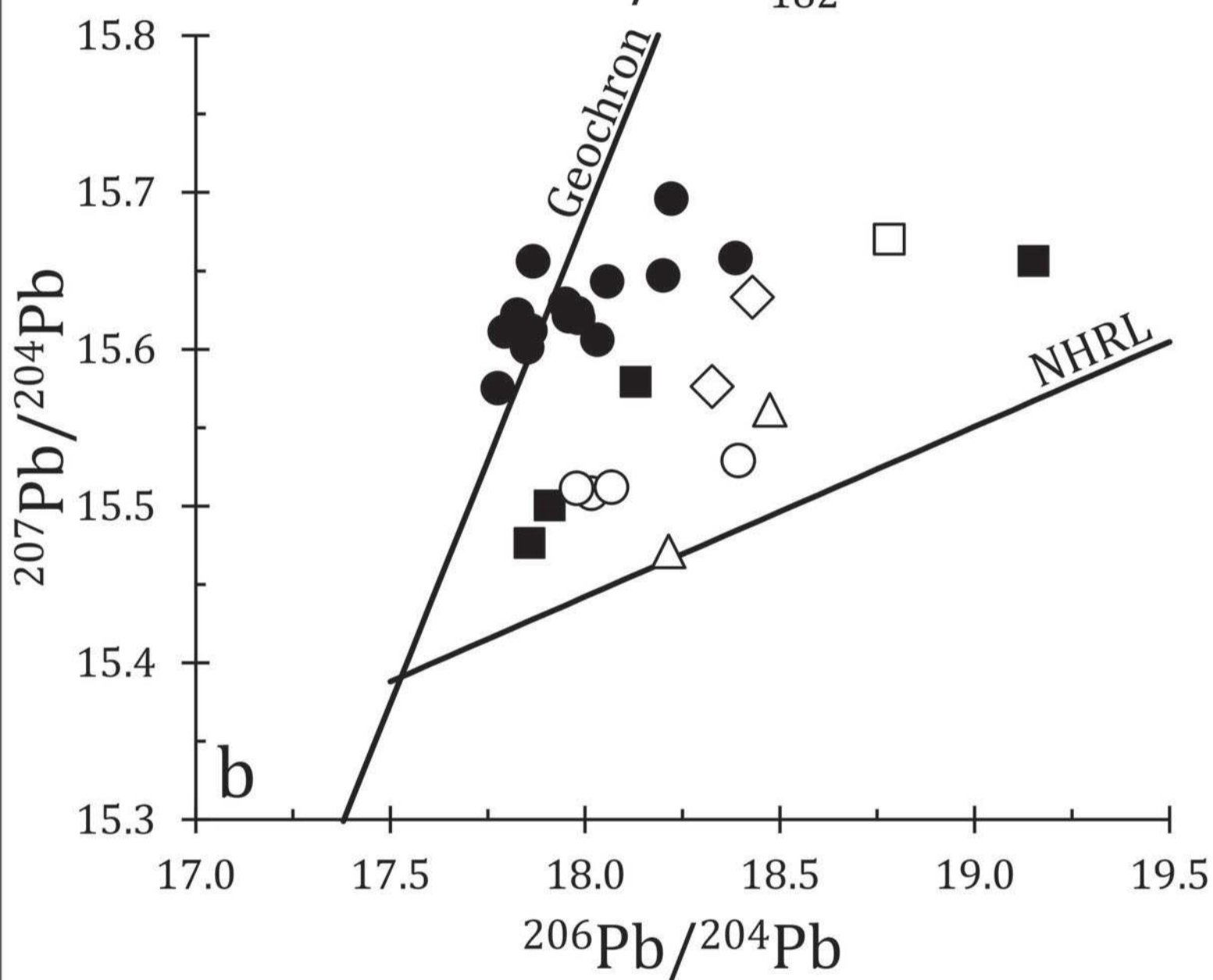
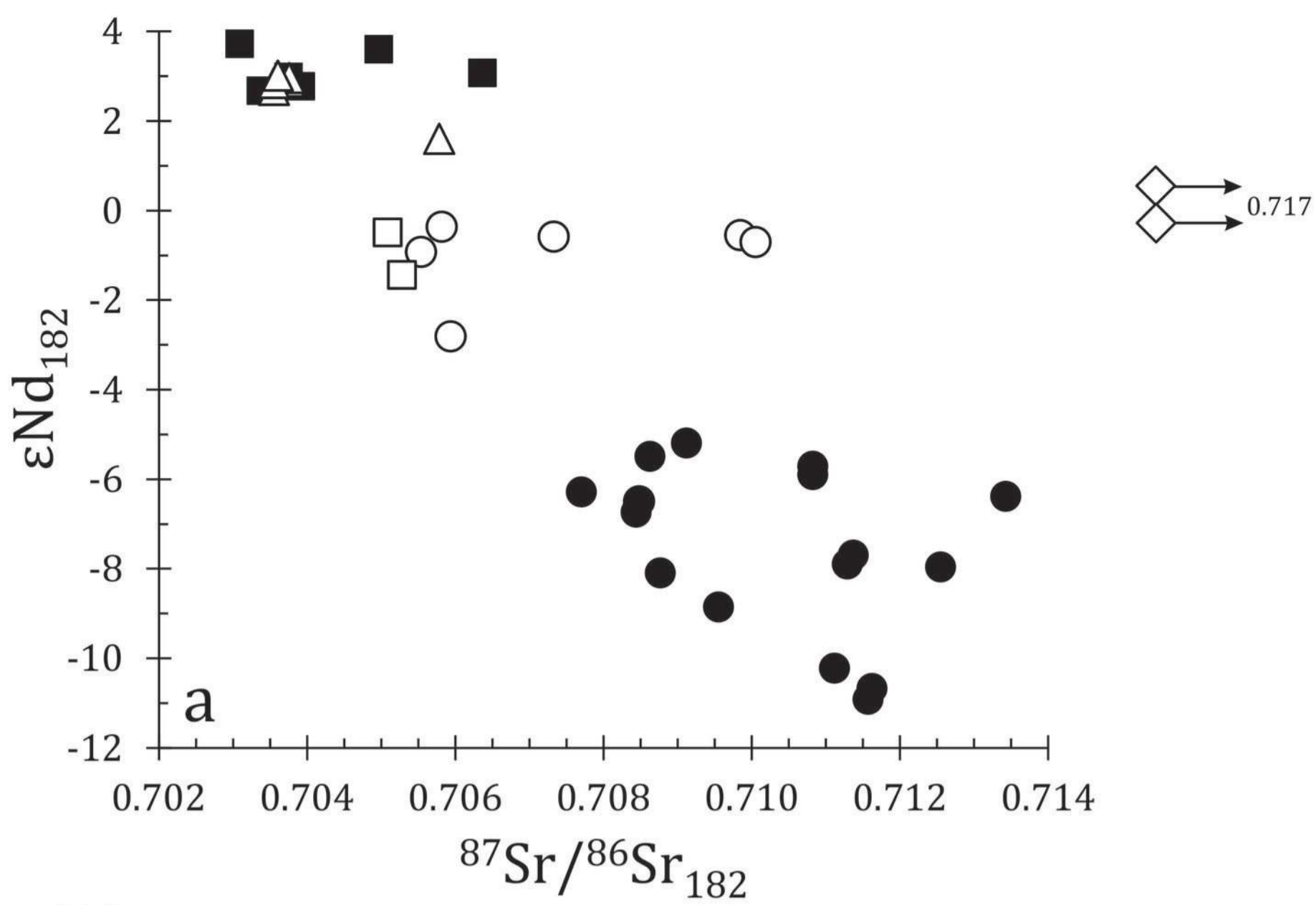
DIT

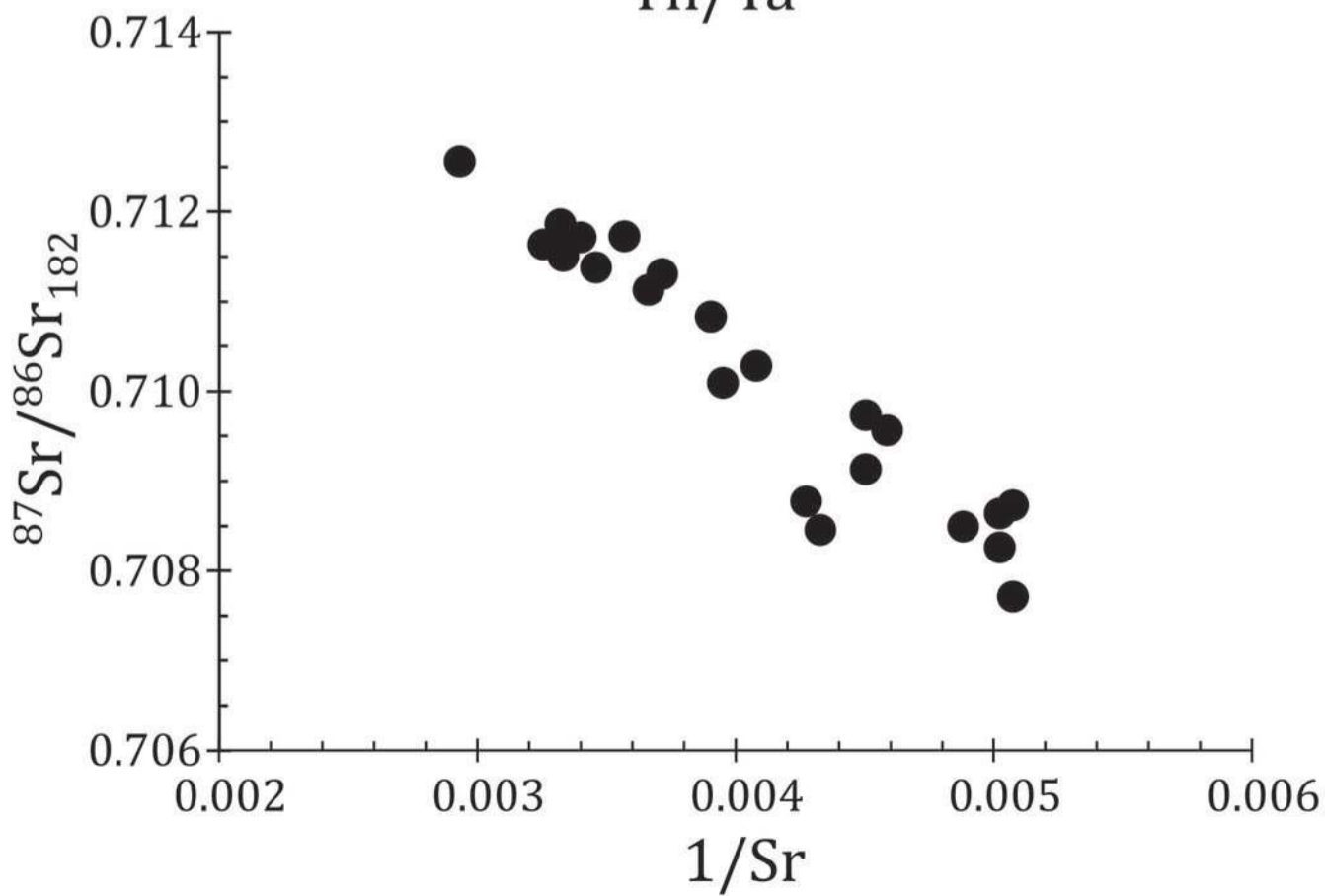
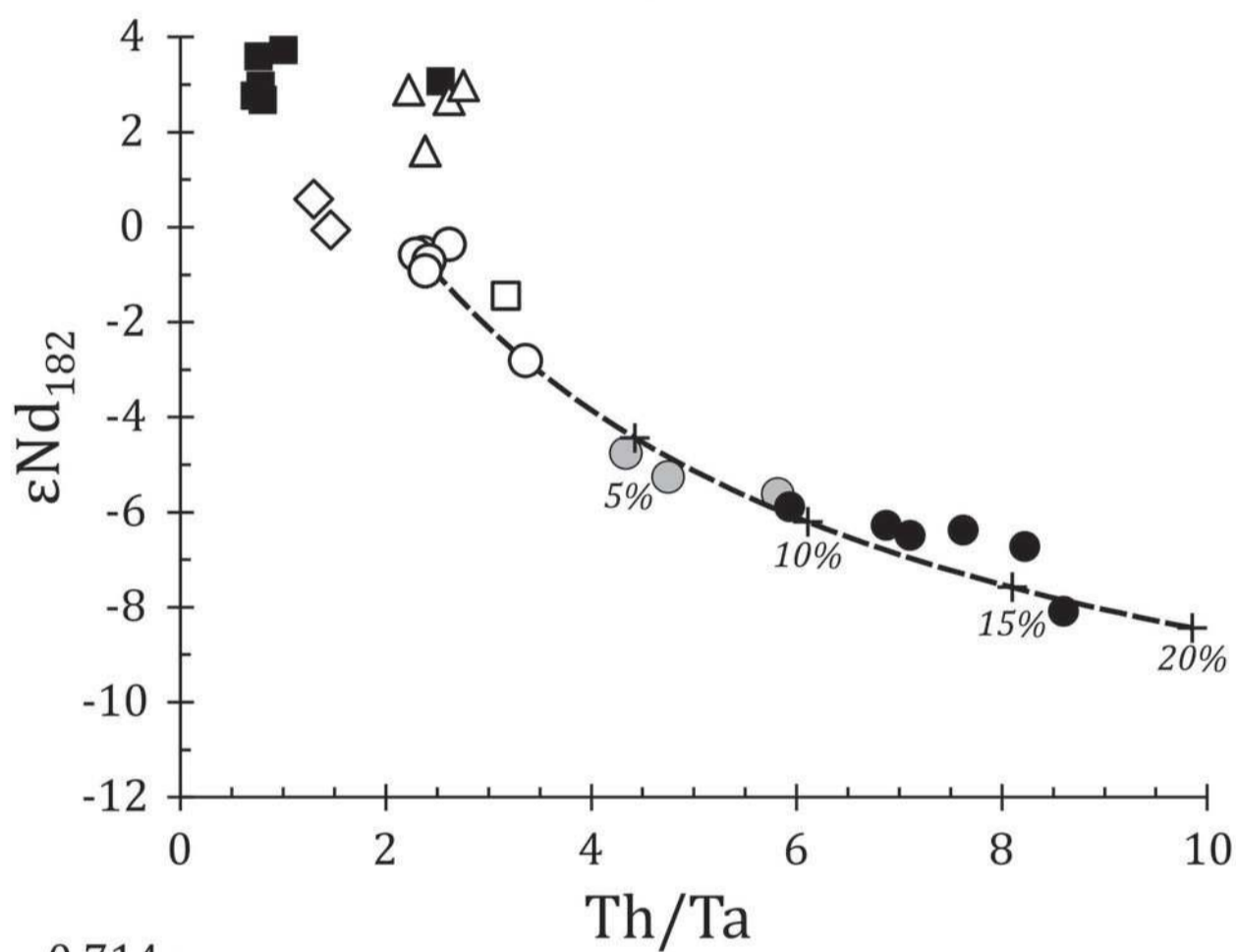
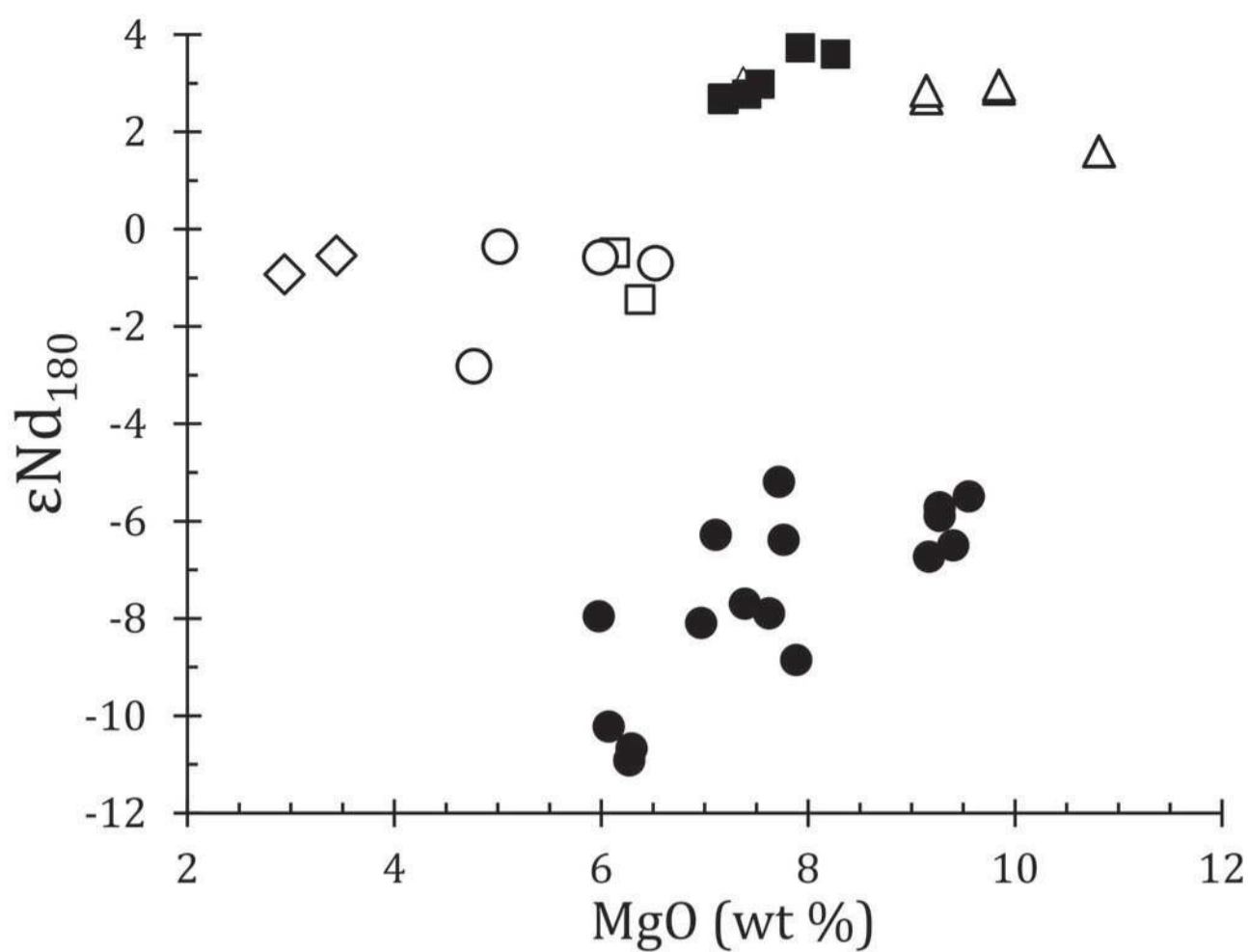
PST

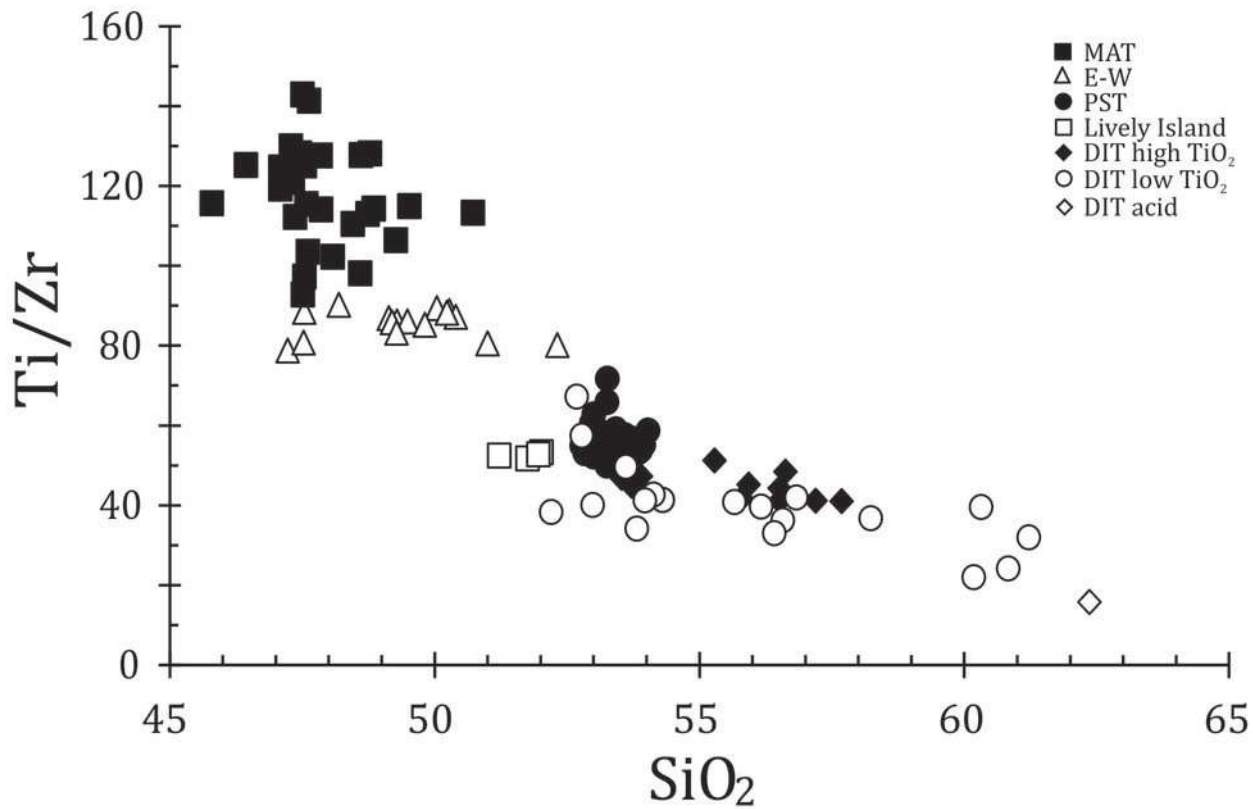


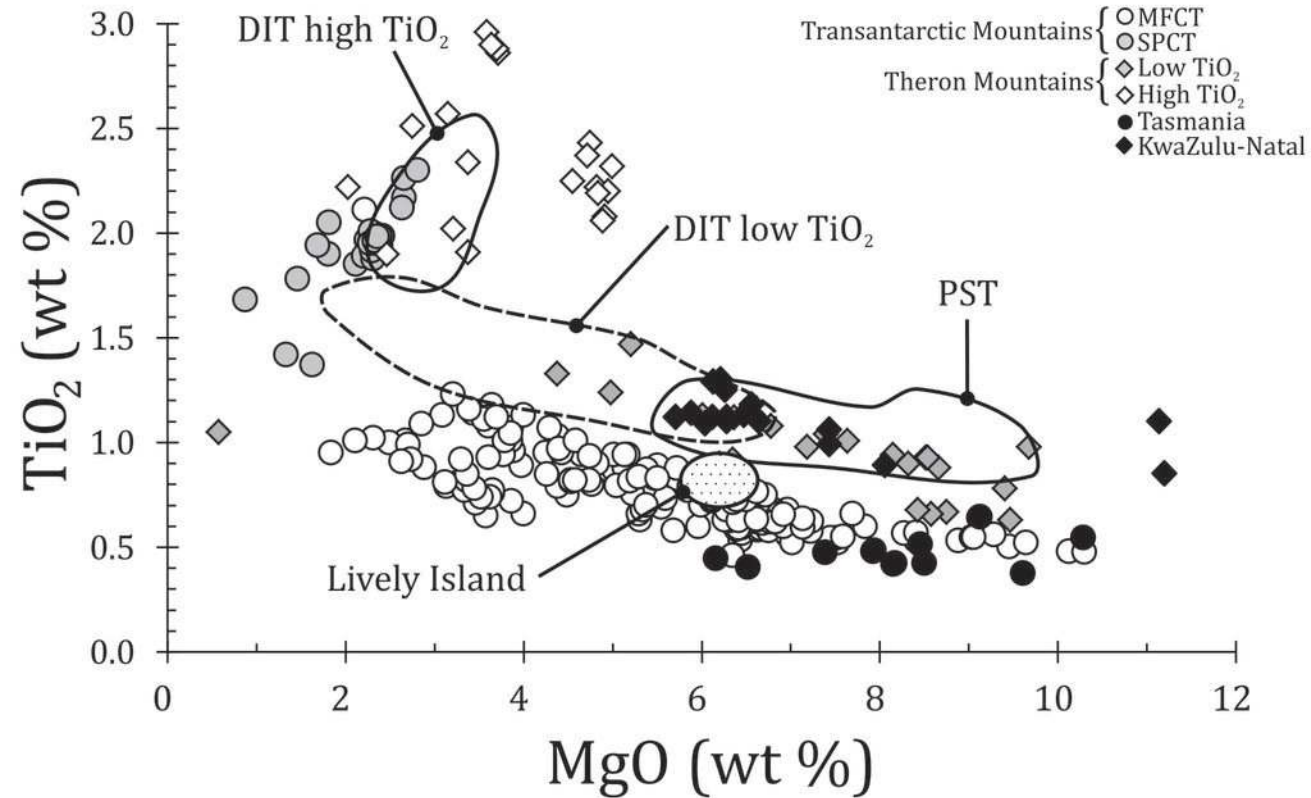


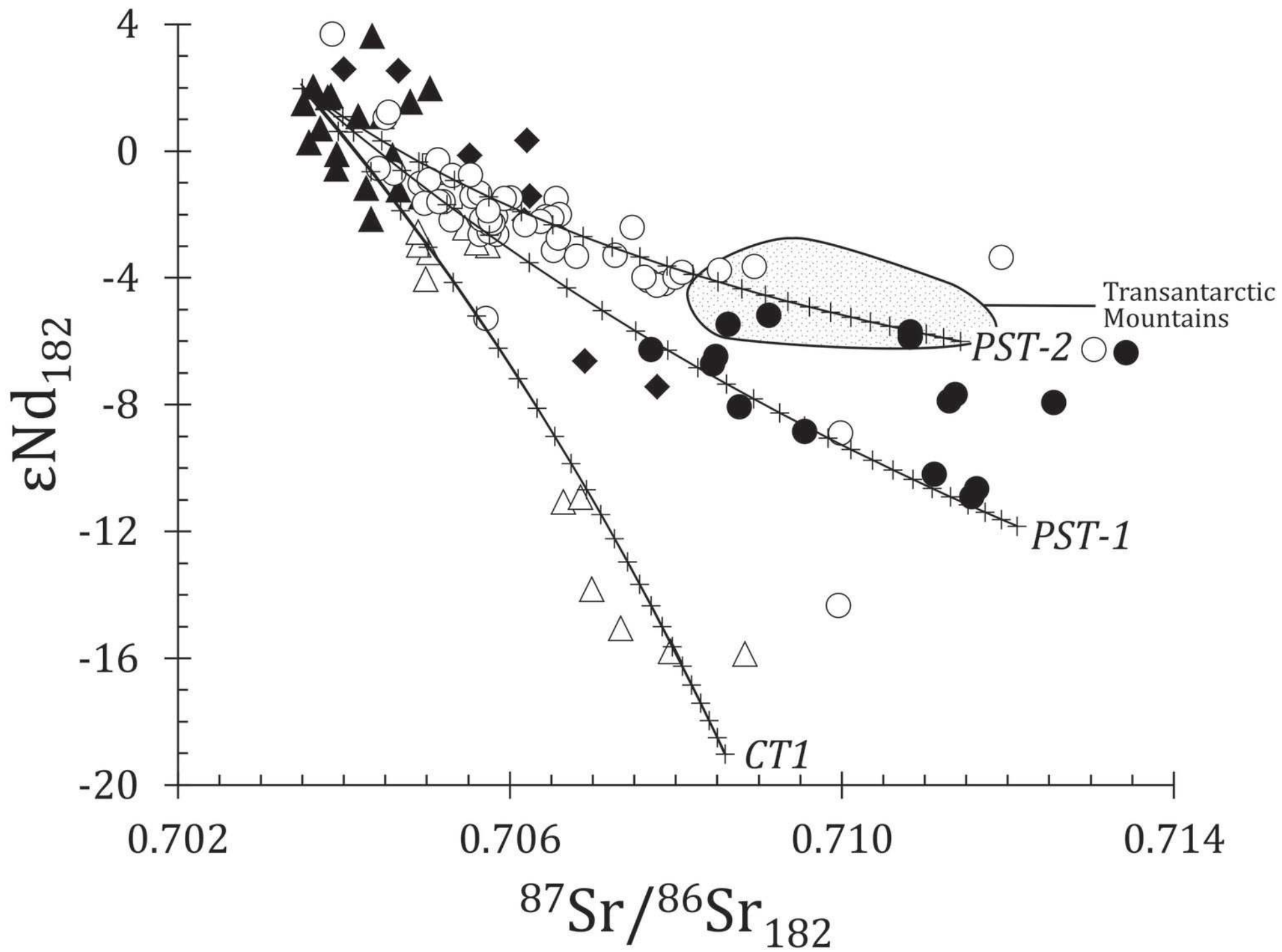


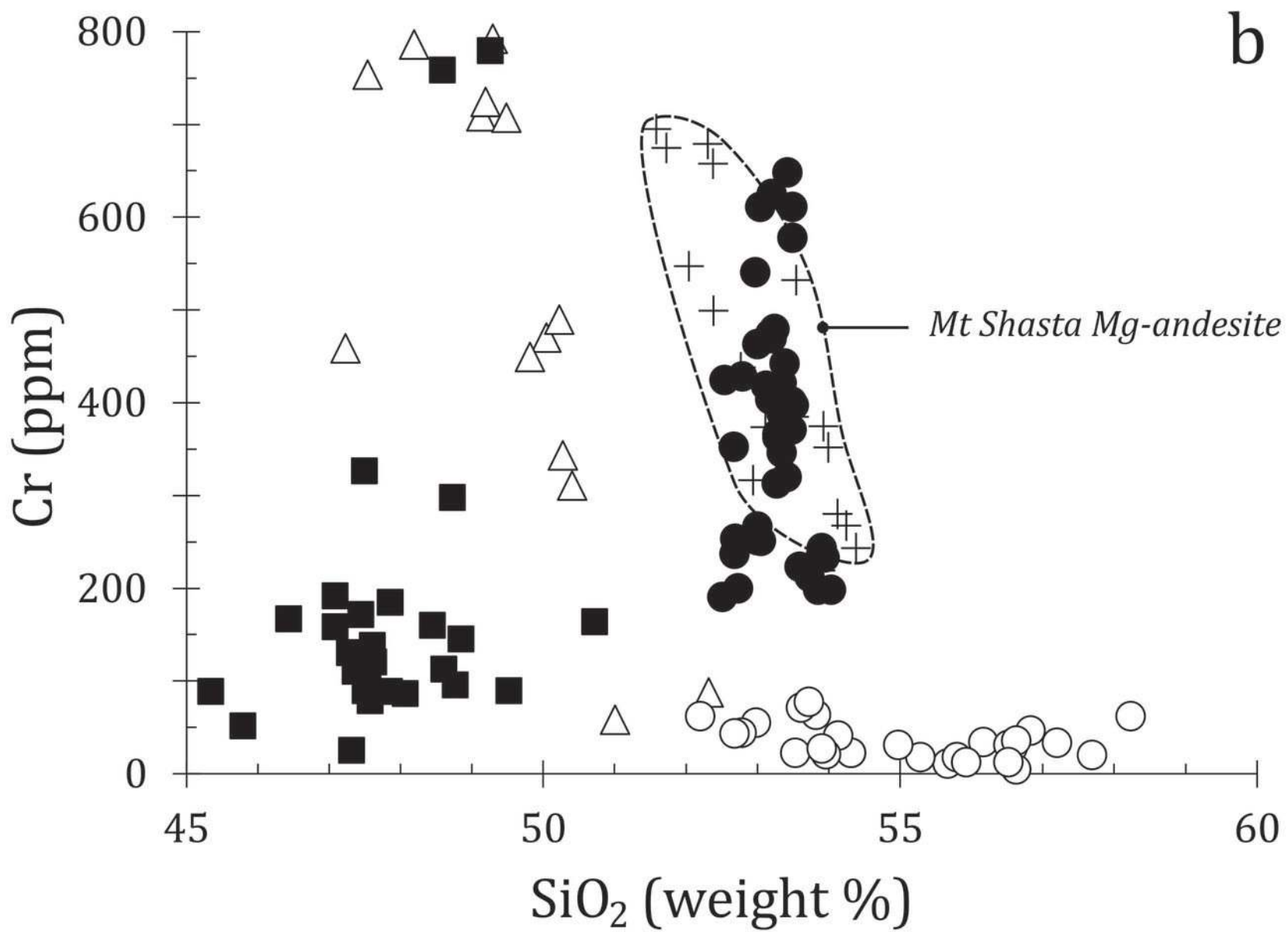
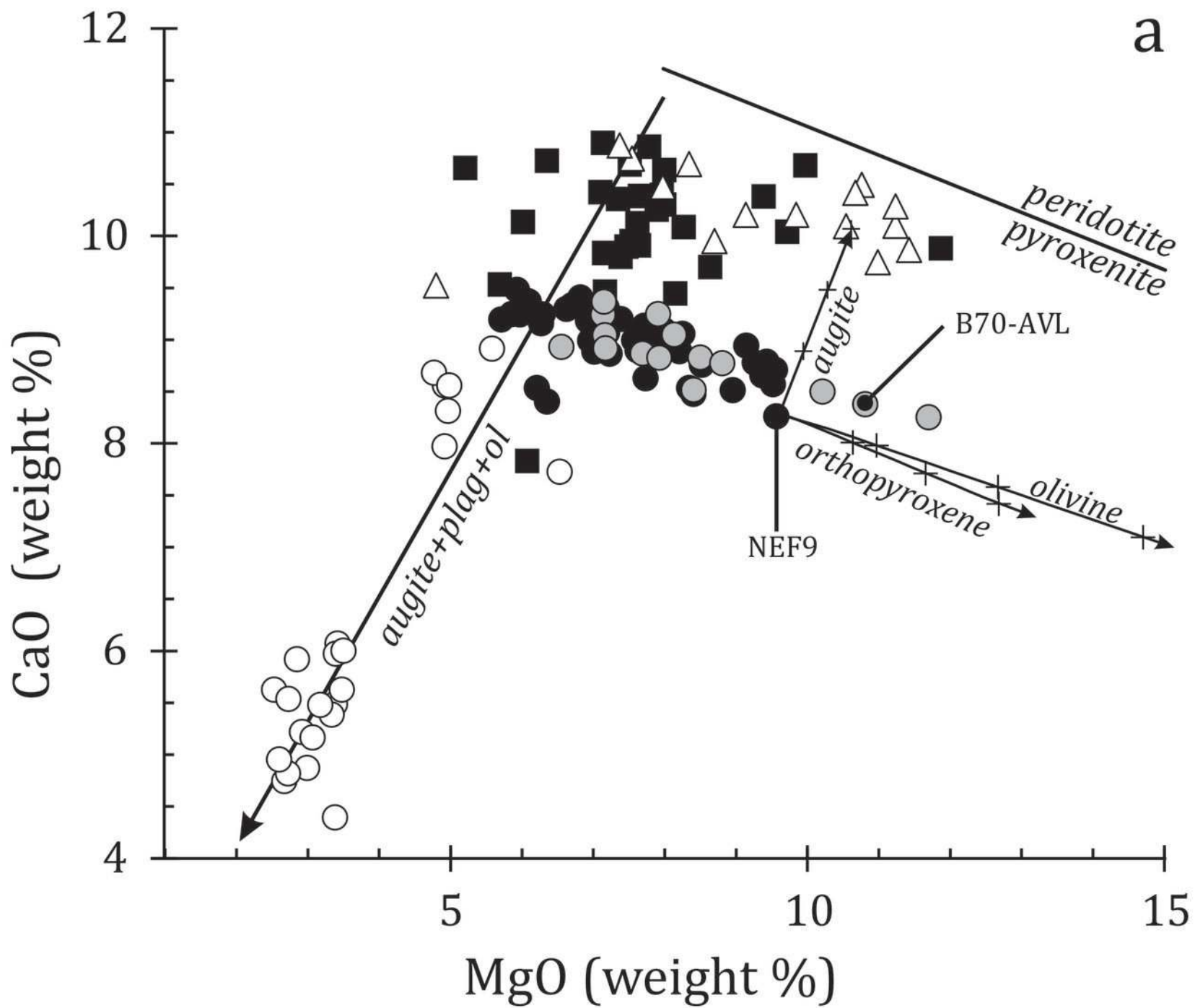


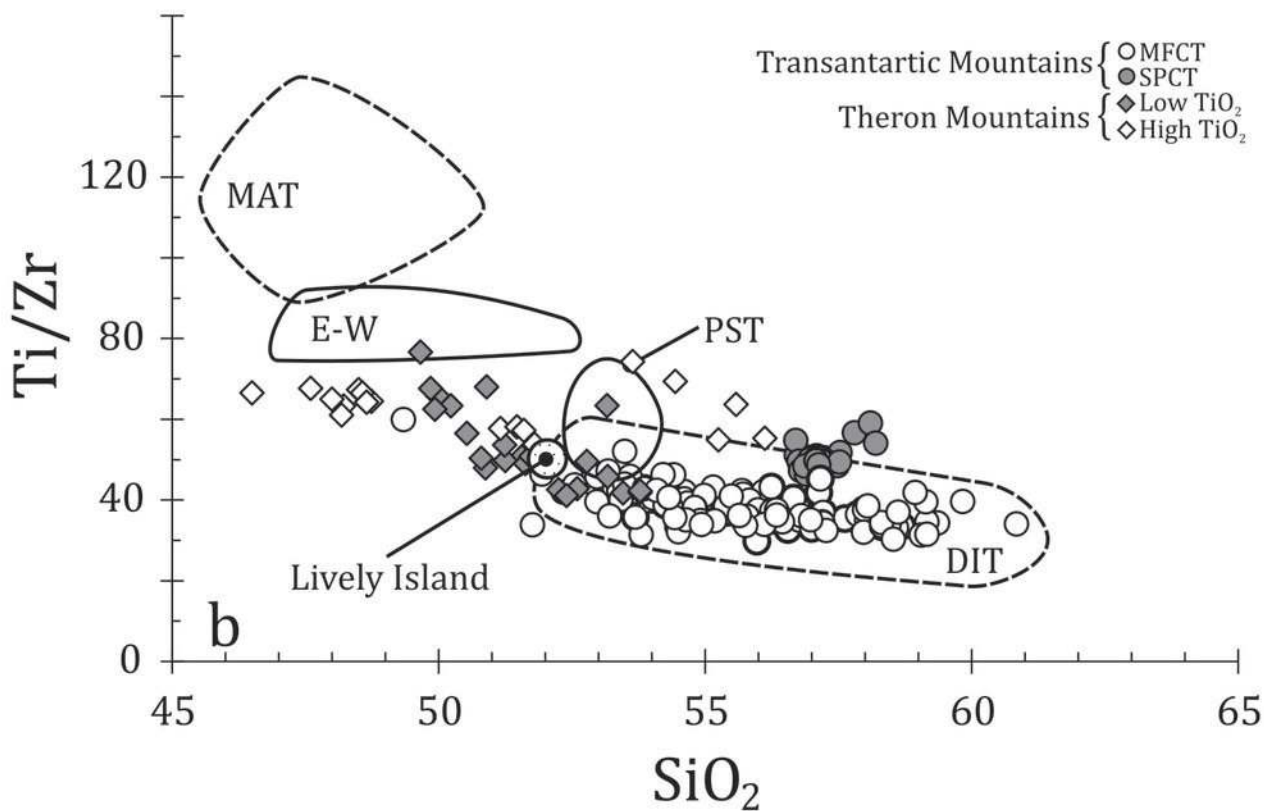
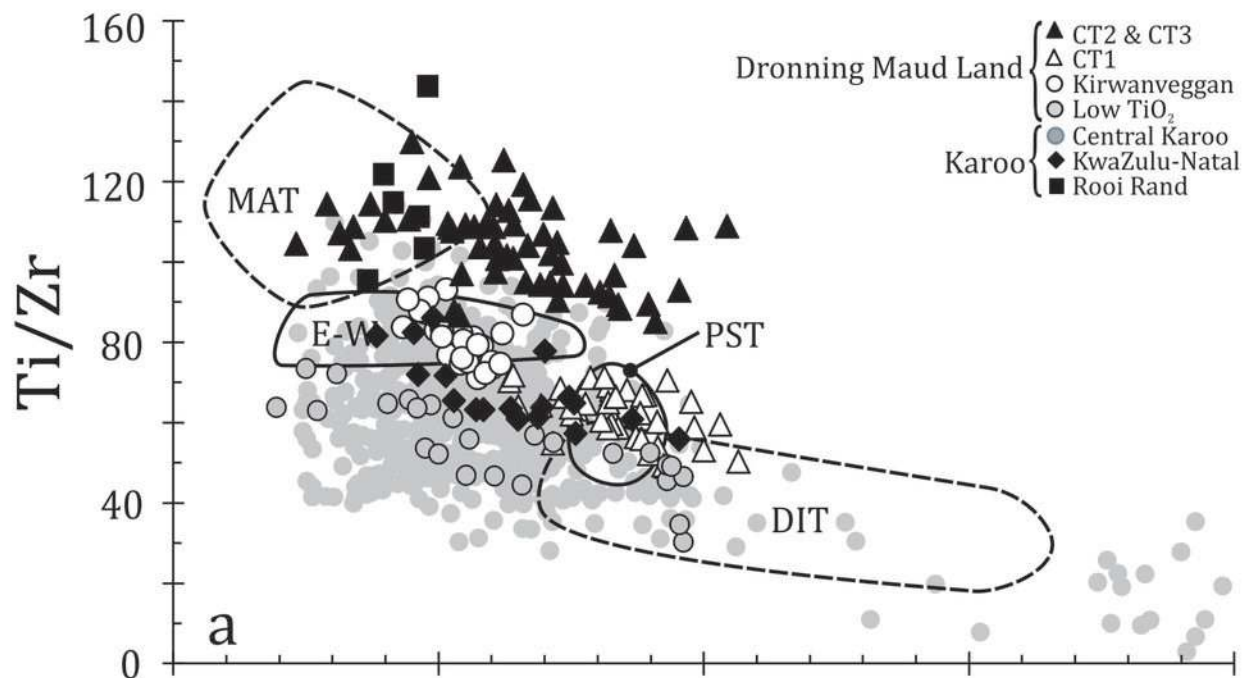


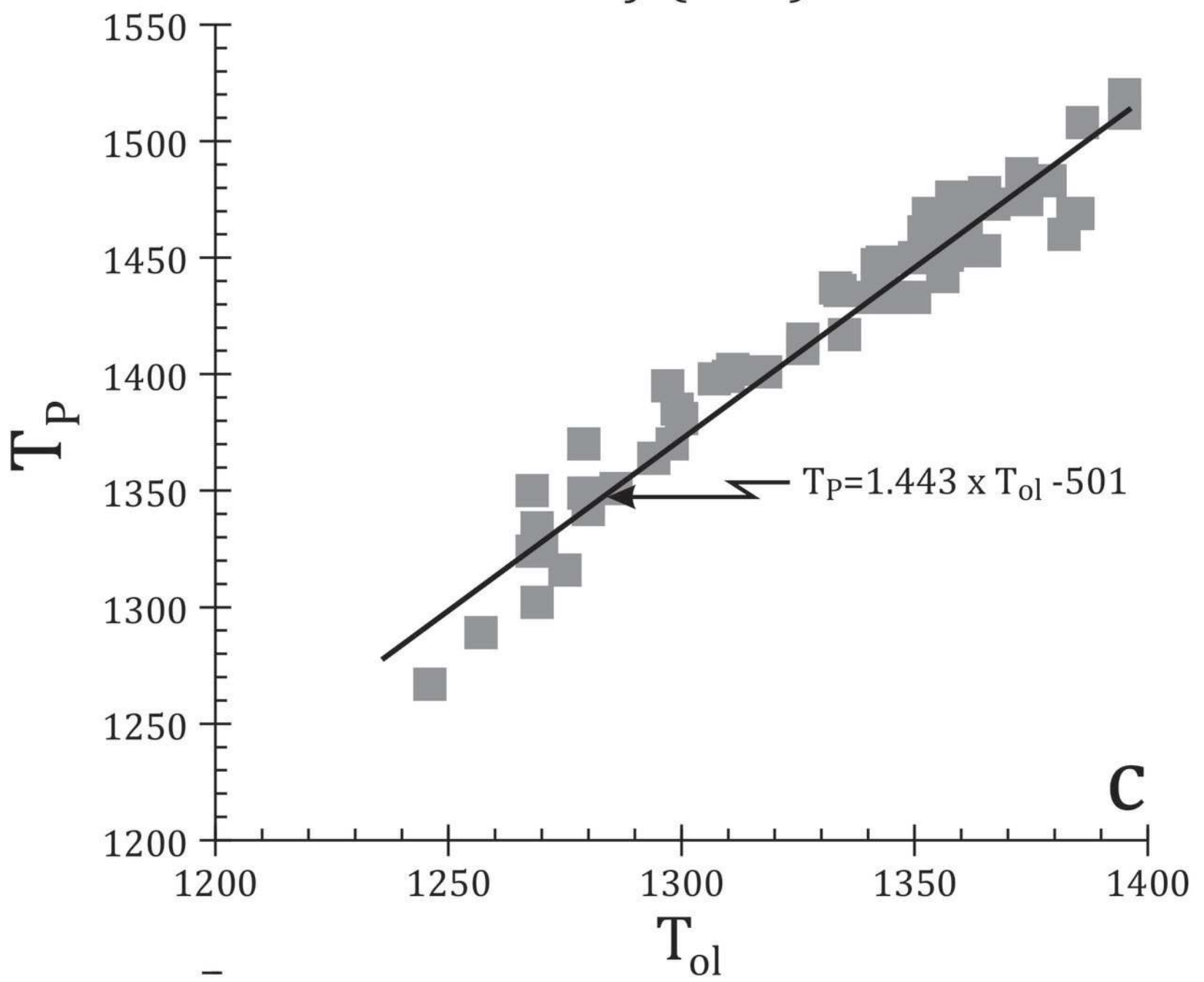
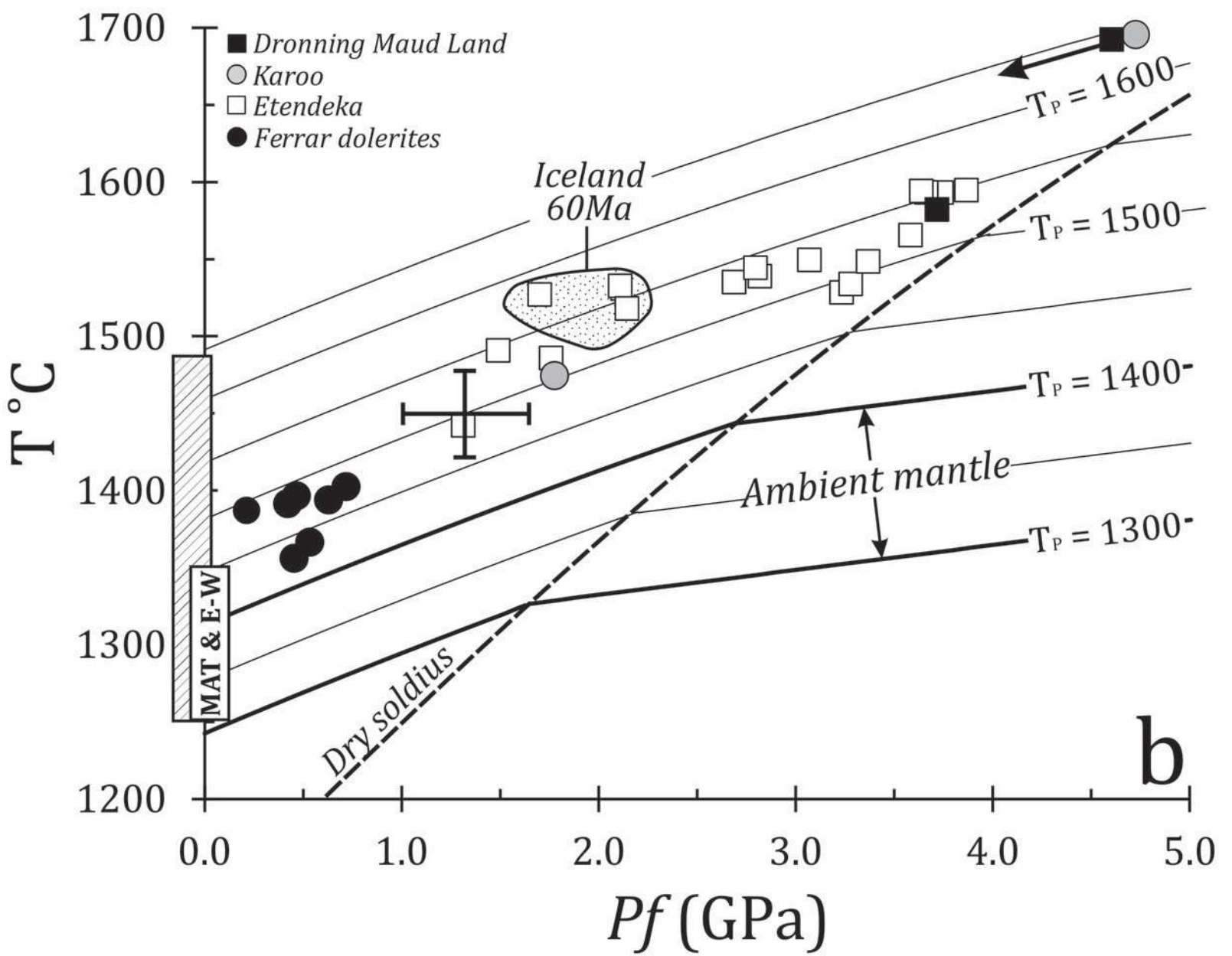
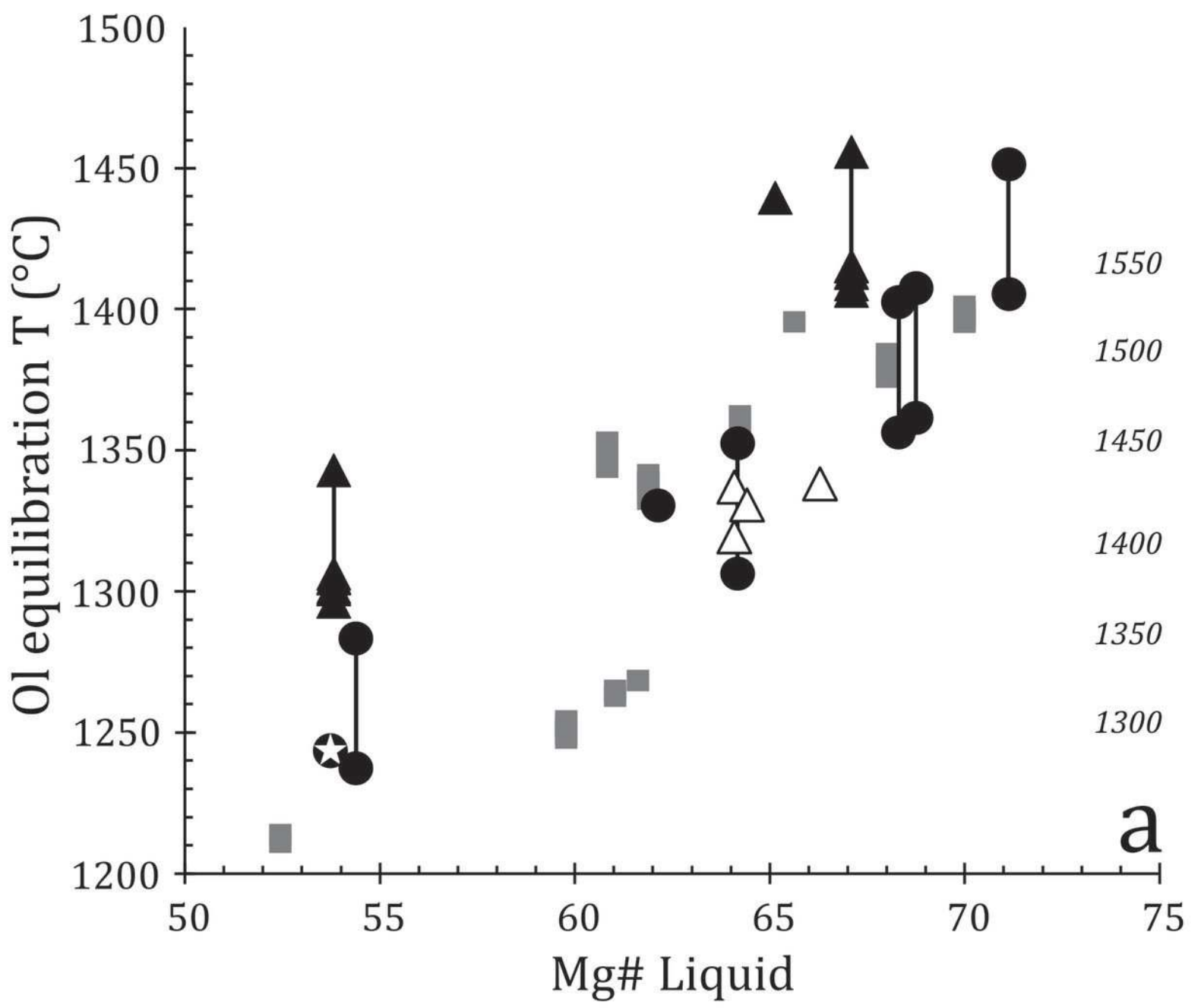












Sample	1187-1	#1503	NEF9	NMF41	MHF1.1	MHF5.5	ECF13	ECF42	ECF44	MHF14.6
Type	PST	PST	PST	PST	PST	PST	EW	EW	EW	EW
SiO ₂	52.67	53.20	52.41	53.59	53.49	53.01	49.49	49.82	50.40	47.02
TiO ₂	0.97	1.02	0.89	1.02	0.99	1.07	1.15	1.21	1.32	0.92
Al ₂ O ₃	14.00	12.90	15.69	14.87	13.15	13.90	14.30	14.47	15.22	14.79
Fe ₂ O ₃	11.94	11.90	11.50	11.25	11.29	12.03	11.91	11.99	11.85	12.54
MnO	0.14	0.14	0.13	0.17	0.13	0.16	0.17	0.18	0.02	0.19
MgO	7.74	9.43	5.96	6.29	9.15	6.93	9.85	9.14	7.38	10.77
CaO	8.63	8.79	9.35	9.24	8.94	9.18	10.20	10.20	10.87	10.49
K ₂ O	2.45	1.90	2.61	2.52	2.10	2.52	2.47	2.58	2.57	2.33
P ₂ O ₅	0.98	0.46	0.77	0.92	0.40	0.55	0.36	0.31	0.26	0.41
Na ₂ O	0.18	0.16	0.16	0.14	0.11	0.13	0.11	0.11	0.11	0.11
TOTAL	99.70	99.90			99.75	99.48				99.57
Loss	1.50	0.50			1.26	2.62				2.20
Rb	33.1	14.2	22	28	17	22	9	9	8	6
Sr	533	205	256	307	232	234	269	282	283	208
Nb	5.8	4.9	6	6	4.3	4.4	6	5	6	6.9
Zr	110	93	97	106	104	113	80	85	91	81
Y	23.9	23.1	25	23	22	25.1	17	19	24	22.1
Cr	352	625	589	223	577	255	707	449	310	458
Ni	100	170	133	75	146	91	236	174	113	254
Ba	nd	nd	1235	365	250	316	167	144	126	208
La	11.6	9.3	9.35	12.42	10.10	12.90	5.54	5.60	6.55	6.9
Ce	25.1	20.1	20.87	27.19	19.90	24.90	14.19	14.29	16.48	13.5
Pr			2.77	3.44			2.09	2.10	2.45	
Nd	14.7	12.3	12.37	14.64	12.00	15.3	10.01	10.16	11.95	8.6
Sm	3.58	3.15	3.29	3.68	3.34	4.06	2.80	2.84	3.37	2.87
Eu	1.22	1.05	1.12	1.19	1.09	1.28	1.03	1.03	1.20	1.01
Gd			3.76	4.16			3.25	3.29	4.10	
Tb	0.72	0.63	0.64	0.68	0.77	0.79	0.54	0.54	0.68	0.67
Dy			3.98	4.20			3.35	3.35	4.42	
Ho			0.80	0.83			0.66	0.67	0.85	
Er			2.30	2.37			1.87	1.90	2.41	
Tm			0.35	0.36			0.28	0.28	0.36	
Yb	2.14	1.93	2.08	2.12	2.09	2.33	1.66	1.68	2.11	2.34
Lu	0.33	0.28	0.31	0.31	0.32	0.36	0.25	0.25	0.31	0.36
Th	1.83	1.35	1.24	2.14	1.48	2.15	0.67	0.60	0.69	1.0
U	0.80	0.50	0.29	0.51	0.5	0.8	0.37	0.24	0.27	0.7
Ta	0.24	0.19	0.21	0.29	0.18	0.25	0.30	0.23	0.25	0.42
Hf	2.73	2.33	2.6	2.86	2.49	3.03	2.05	2.27	2.48	2.01
Pb			5.55	4.93			2.19	2.65	2.65	
Cs	0.42	0.29			2.24	0.74				0.3
Co	43.30	47.30			50.8	42.9				61.4
Sc	25.70	26.60			27.8	28.2				35
⁸⁷ Sr/ ⁸⁶ Sr	0.71448	0.70900			0.70900	0.70948				0.70600
± 2SE	±1	± 2			± 18	± 17				±2
⁸⁷ Sr/ ⁸⁶ Sr ₁₈₂	0.71343	0.70848	0.71083		0.70845	0.70877	0.70579	0.70376	0.70355	0.70578
¹⁴³ Nd/ ¹⁴⁴ Nd	0.512252	0.512255			0.512259	0.512181				0.512726
± 2SE	±7	±5			± 6	± 6				±7
¹⁴³ Nd/ ¹⁴⁴ Nd ₁₈₂	0.512069	0.512063	0.512367		0.51205	0.511981	0.512561	0.512551	0.512565	0.512475
εNd ₁₈₂	-6.4	-6.5	-5.7		-6.7	-8.1	2.9	2.7	3.0	1.6
²⁰⁶ Pb/ ²⁰⁴ Pb		17.826±11	17.86		18.394±8	18.057± 7		18.21		18.474±7
²⁰⁷ Pb/ ²⁰⁴ Pb		15.622±8	15.61		15.658± 8	15.643±8		15.47		15.561±8
²⁰⁸ Pb/ ²⁰⁴ Pb		38.044±19	37.97		38.143±20	38.246±16		37.58		38.111±15
Sample	1187-1	#1503	NEF9	NMF41	MHF1.1	MHF5.5	ECF13	ECF42	ECF44	MHF14.6

Sample	MHF25.1	FAR338	WI-5	MHF18.3	NHF17	MHF14.9	MHF44.1	WI-3	MHF18.1	MHF41.3
Type	Lively	DIT	DIT	DIT	DIT	DIT	DIT Acid	DIT Acid	DIT Acid	DIT Acid
SiO ₂	51.76	52.41	52.44	53.24	53.97	56.06	55.49	60.88	64.11	68.92
TiO ₂	0.82	0.89	1.10	1.30	1.32	1.81	1.54	1.63	1.51	0.71
Al ₂ O ₃	15.94	15.69	19.53	15.01	13.27	14.30	15.28	15.24	15.96	15.03
Fe ₂ O ₃	10.33	11.5	8.66	12.05	13.88	12.28	12.31	9.19	10.61	6.57
MnO	0.13	0.13	0.12	0.12	0.22	0.18	0.22	0.12	0.06	0.10
MgO	6.38	5.96	6.54	4.99	4.77	2.93	3.48	1.96	1.67	0.60
CaO	11.27	9.35	7.73	8.56	8.68	5.22	5.63	3.01	0.75	0.40
K ₂ O	2.46	2.61	2.92	3.21	2.52	4.10	3.76	5.74	3.25	3.51
P ₂ O ₅	0.73	0.77	0.22	0.66	1.18	2.06	1.78	1.10	0.75	3.29
Na ₂ O	0.17	0.16	0.11	0.17	0.19	0.25	0.20	0.59	0.69	0.21
TOTAL	99.63	99.49	99.36	99.30		99.20	99.69	99.45	99.36	99.34
Loss	1.88	2.10	3.28	3.64		4.12	1.56	2.81	3.30	3.44
Rb	10.9	21.7	29	17.6	34	40.8	40	18.2	20.5	59.6
Sr	231	493.3	582	367	178	358	324	302	1204	715
Nb	10.3	9.1	9.5	12.0	16	18.2	27.4	35.2	74.4	72
Zr	93	96	115	158	192	267	226	309	502	620
Y	21.4	20.0	21.8	30.0	39	41.1	36.2	48.2	85.5	64.8
Cr	172	43	44	71	21	31	11	15	13	19
Ni	63	-	7	95	10	20	6	2.0	8	2.0
Ba	205	494	153	199	371	1409	528	207	2939	862
La	10.8	11.7	16.0	15.7	21.36	26.7	27.0	42.8	47.5	68.9
Ce	21.3	24.1	33.9	32.6	48.50	58.3	55.6	91.9	108	140.0
Pr					6.14					
Nd	11.9	14.7	19.2	20.5	25.93	36.4	29.7	47.0	58.9	69.3
Sm	2.9	3.39	4.41	5.32	6.12	7.92	6.18	10.4	13.2	13.60
Eu	0.92	1.14	1.34	1.63	1.72	2.25	1.77	2.55	3.09	3.41
Gd					6.46					
Tb	0.61	0.60	0.73	0.94	1.07	1.27	1.04	1.55	2.07	2.06
Dy					6.62					
Ho					1.34					
Er					3.91					
Tm					0.62					
Yb	2.41	1.82	2.43	2.81	3.74	3.97	3.62	5.11	7.07	7.47
Lu	0.4	0.28	0.37	0.44	0.056	0.60	0.55	0.76	1.05	1.11
Th	1.68	1.03	1.50	1.49	3.19	2.48	3.90	5.17	5.6	6.54
U	0.8		0.90	0.9	0.77	1.20	1.30	1.70	2.2	2.10
Ta	0.53	0.45	0.62	0.57	0.95	1.04	1.54	2.19	4.32	4.47
Hf	2.32	2.24	3.18	3.78	5.29	5.94	5.53	8.35	11.7	13.80
Pb					13.83					
Cs	0.47		0.28	0.4		0.56	0.38	0.20	0.3	0.20
Co	39.3	21.5	23.20	50.6		35.00	29.4	16.70	12.5	7.40
Sc	37.4	17.1	18.80	15.8		24.70	23.7	18.40	16.3	13.30
⁸⁷ Sr/ ⁸⁶ Sr	0.70564	0.70771±1	0.71042	0.70618		0.70730	0.70730	0.71029	0.71720	0.71745
± 2SE	±15	1	±6	±17		± 17	± 17	± 23	±17	±14
⁸⁷ Sr/ ⁸⁶ Sr ₁₈₂	0.70510	0.70733	0.71004	0.70581	0.70594	0.70554	0.70637	0.70983	0.71716	0.71714
¹⁴³ Nd/ ¹⁴⁴ Nd	0.512505	0.512540±	0.512533 ±8	0.512572		0.512561	0.512561	0.512535	0.512595	0.512542
± 2SE	±8	9		±5		± 6	± 6	± 7	±7	±7
¹⁴³ Nd/ ¹⁴⁴ Nd ₁₈₂	0.512322	0.512374	0.51236	0.512377	0.512259	0.512349	0.512405	0.512369	0.512427	0.512398
εNd ₁₈₂	-1.5	-0.6	-0.7	-0.4	-2.8	-0.9	3.1	-0.6	0.6	-0.1
²⁰⁶ Pb/ ²⁰⁴ Pb	18.781±9	17.980±9	18.067±9	18.430±8				18.016±10	18.326±8	18.393±6
²⁰⁷ Pb/ ²⁰⁴ Pb	15.670±9	15.510±8	15.512±8	15.633±7				15.508±10	15.576±8	15.529±6
²⁰⁸ Pb/ ²⁰⁴ Pb	38.300±23	37.361±18	37.425±12	37.944±2				37.492±26	37.880±20	37.583±12

Sample	MHF15.2	MHF14.4	MHF15.1	MA1
Type	MAT	MAT	MAT	MAT
SiO ₂	45.92	47.40	48.56	47.51
TiO ₂	1.81	1.52	1.71	1.39
Al ₂ O ₃	15.70	16.39	16.71	16.45
Fe ₂ O ₃	13.60	13.23	12.52	12.91
MnO	0.16	0.17	0.21	0.20
MgO	8.00	7.51	7.15	8.27
CaO	10.59	10.65	9.80	10.05
K ₂ O	2.59	2.53	2.53	2.65
P ₂ O ₅	0.30	0.05	0.17	0.38
Na ₂ O	0.20	0.17	0.19	0.20
TOTAL	98.87	99.63	99.56	
Loss	1.5	1.90	2.25	
Rb	4.7	5.5	2.0	10
Sr	424	444	381	396
Nb	11.2	9.9	10.7	7
Zr	80	79	80	90
Y	21.1	18.6	18.2	19
Cr	89	78	95	89
Ni	119	102	121	116
Ba	110	105	103	827
La	8.1	8.0	7.9	4.37
Ce	18.0	17.2	18.3	11.45
Pr				1.83
Nd	13.3	12.8	13.8	9.73
Sm	3.72	3.32	3.78	3.08
Eu	1.38	1.25	1.42	1.29
Gd				3.72
Tb	0.7	0.63	0.72	0.61
Dy				3.66
Ho				0.71
Er				1.97
Tm				0.30
Yb	2.05	1.83	2.04	1.69
Lu	0.32	0.28	0.33	0.23
Th	0.42	0.42	0.48	0.26
U				0.09
Ta	0.58	0.54	0.6	0.3
Hf	2.28	1.94	2.26	2.60
Pb				1.07
Cs	0.3	0.35	0.2	
Co	48.2	42.60	49.3	
Sc	28.9	25.40	28.6	
⁸⁷ Sr/ ⁸⁶ Sr	0.70400	0.70385±17	0.70342	
± 2SE	±14		±15	
⁸⁷ Sr/ ⁸⁶ Sr ₁₈₂	0.70392	0.70375	0.70338	0.70497
¹⁴³ Nd/ ¹⁴⁴ Nd	0.512747	0.512743	0.512738	
± 2SE	±6	±17	±6	
¹⁴³ Nd/ ¹⁴⁴ Nd ₁₈₂	0.512537	0.512548	0.512532	0.512588
εNd ₁₈₂	2.8	3.0	2.7	3.6
²⁰⁶ Pb/ ²⁰⁴ Pb	19.152±6	17.858±7	18.131±7	17.91
²⁰⁷ Pb/ ²⁰⁴ Pb	15.656±5	15.476±6	15.579±7	15.50
²⁰⁸ Pb/ ²⁰⁴ Pb	38.464±13	37.425±18	37.762±16	37.57

Table 1. Whole-rock major and trace element and isotopic compositions of Falkland Islands intrusions used in this study. Major elements and isotopic compositions for sample numbers starting with EC, NE, NH, NM and MA are from Mitchell *et al.* (1999) with addition trace elements from this study. See supplementary materials for analytical methods.

Table 2. Geochemical, mineralogical and petrographical characteristics of the different groups of Falkland Islands intrusions.

Type	Type locality	Mitchell ¹	Stone ²	Petrographic features	Mineralogy	Subgroup	Mg#	SiO ₂	TiO ₂	Ti/Zr	Zr/Y	⁸⁷ Sr/ ⁸⁶ Sr ₁₈₂	εNd ₁₈₂
Port Sussex Creek (PST)	Port Sussex 51°40'15" S 58°58'41" W	N-S	NE-SW	Coarse-grained dolerite	Pig ± Opx + Aug Rare Ol + Di	none	48-58	52-54	0.9-1.2	50-70	3.6-5.3	0.7077-0.7134	-5.5 to -10.9
E-W	Fox Bay West 51°57'02" S 60°05'21" W	E-W	E-W	Coarse-grained olivine dolerite	Ol + Plag ± Aug	none	42-64	47-54	1.0-1.9	77-90	3.2-4.8	0.7036-0.7058	-0.4 to +3.0
Lively Island (LI)	Lively Island 52°00'00" S 58°27'47" W	Lively Island	NE-SW	Coarse-grained with accessory biotite	Ol + Plag + Aug ± rare pigeonite	none	48-52	51-52	0.8-0.9	53	4.0-4.54	0.7053	-0.5 to -1.4
Dyke Island (DIT)	Dyke Island 51°59'33" S 60°52'50" W	Not defined	Radial swarm	Fine-grained aphyric, rarely plagioclase ± augite-phyric	Plag + Aug	Acid	<22	62-75	0.2-1.6	<31	5.0-8.8	0.7055-0.7098	-2.8 to -0.5
						Low TiO ₂	27-57	52-61	1.1-1.7	24-67	4.8-7.4		
						High TiO ₂	41-51	53-58	>1.80	25-53	6.8-8.4		
Mount Alice (MAT)	Mount Alice 52°09'12" S 60°35'55" W	Mount Alice	Radial swarm	Fine-grained plagioclase ± olivine phyric	Ol + Plag ± Aug	none	44-64	47-50	1.3-1.9	98-142	3.2-5.2	0.7031-0.7039	0.0 to +3.7

1. Groups described by Mitchell *et al.* (1999); 2. Groups defined by Stone *et al.* (2009)

Calculated extract for fractionation of PST and E-W intrusions

	PST			E-W		
	NGF16	MHF5.1	Calc	ECF12	ECF44	Calc
SiO ₂	54.01	53.81	53.82	49.69	51.03	50.98
TiO ₂	0.94	1.00	1.13	1.05	1.21	1.36
Al ₂ O ₃	13.20	14.97	15.02	13.30	15.21	15.20
FeO	10.60	10.62	10.60	10.51	11.11	11.06
MnO	0.20	0.17	0.18	0.17	0.17	0.21
MgO	9.67	6.78	6.78	11.62	6.71	6.70
CaO	8.81	9.50	9.49	9.81	11.51	11.50
Na ₂ O	1.96	2.62	2.56	2.29	2.56	2.46
K ₂ O	0.48	0.42	0.56	0.32	0.39	0.39
P ₂ O ₅	0.12	0.11	0.15	0.11	0.11	0.13
Extract			%			%
Olivine		Fe ₈₃	0.0			57.0
Plagioclase		An ₇₀	18.9			40.4
Pyroxene		En ₇₁ Fe ₁₉ Wo ₉	74.7			
Pyroxene		En ₅₁ Fe ₁₃ Wo ₃₃	6.4			2.6
Σ residuals ²			0.127			0.038
F			0.79			0.75

Table 4 AFC parameters for the trajectories shown in Fig. 12. R is the ratio of assimilated rock to crystal cumulate. A value appropriate for upper-crustal contamination has been used. F is the total amount of crystallization required to reach the most extreme composition on a particular trajectory. T_{CHUR} is the Chondritic Uniform Reservoir model Nd age for the most extreme composition on a particular trajectory, in Ga.

		AFC parameters								T_{CHUR}
		Sr	Nd	ϵNd	$^{87}\text{Sr}/^{86}\text{Sr}$	D_{Sr}	D_{Nd}	R	F	(Ga)
CT1	Source	50	5	2	0.7035	0.5	0.1	0.40	≤ 0.2	3.0
	Crust	400	20	-50	0.7120					
PST-1	Source	60	4	2	0.7035	0.5	0.1	0.40	≤ 0.2	2.2
	Crust	350	40	-20	0.7200					
PST-2	Source	100	5	2	0.7035	0.5	0.1	0.40	≤ 0.2	1.8
	Crust	350	60	-10	0.7250					